CHALMERS
UNIVERSITY OF TECHNOLOGY

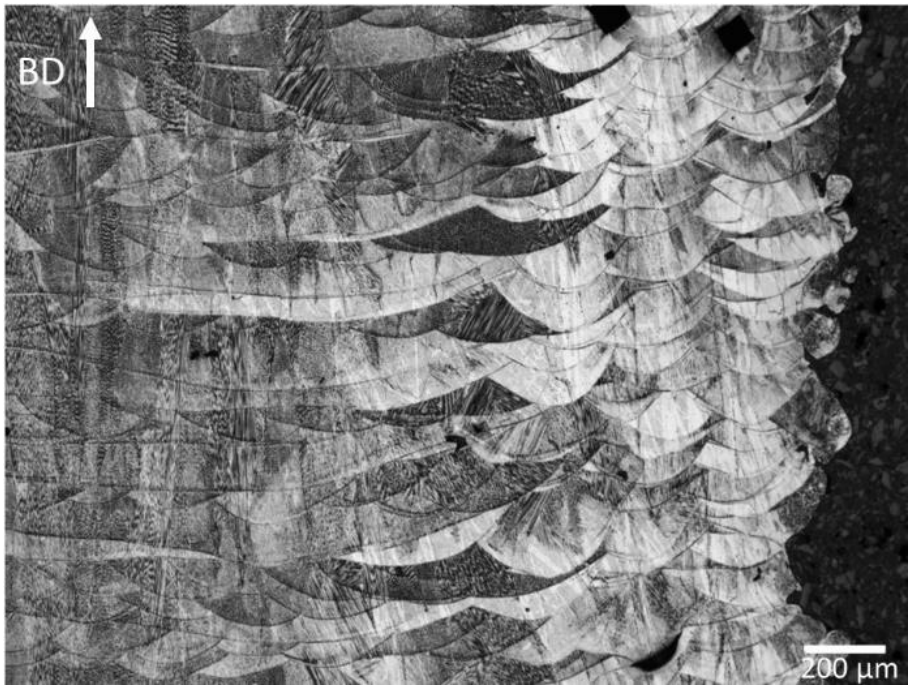

Surface integrity analysis before and after machining of additively manufactured (3D printed) 316L stainless steel using Selective Laser Melting (SLM) and Electron Beam Melting (EBM)

MASTER'S THESIS WORK IN MATERIALS ENGINEERING

AMIR REZA SHAHAB

Department of Industrial and Materials Science
Chalmers University of Technology
Gothenburg, Sweden 2020

CHALMERS
UNIVERSITY OF TECHNOLOGY

MASTER'S THESIS 2020:06

Surface integrity analysis before and after machining of additively manufactured (3D printed) 316L stainless steel using Selective Laser Melting (SLM) and Electron Beam Melting (EBM)

Master's Thesis in Materials Engineering

Amir Reza Shahab

Department of Industrial and Materials Science

Division of Materials and Manufacture

CHALMERS UNIVERSITY OF TECHNOLOGY

Gothenburg, Sweden- June 2020

CHALMERS
UNIVERSITY OF TECHNOLOGY

Surface integrity analysis before and after machining of additively manufactured (3D printed) 316L stainless steel using selective laser melting (SLM) and electron beam melting (EBM)

AMIR REZA SHAHAB

Master's thesis work in materials engineering master's program

© AMIR REZA SHAHAB, 2020

Supervisor at RISE AB: Seyed Behnam Hosseini

Supervisor at Chalmers: Dinesh Mallipeddi

Examiner: Uta Klement, Industrial and Materials Science

Master's thesis 2020

Department of Industrial and Materials Science

Division of Materials and Manufacture

Chalmers University of Technology

SE-41296 Gothenburg

Telephone: +46736325001- Email: arshahab81@gmail.com

This project was performed in a collaboration between Chalmers University of Technology (CAM2 Center of Additive Manufacturing) and RISE Research Institute of Sweden.

Cover image: The image shows the microstructure of 316L produced by electron beam melting (EBM)

Gothenburg, Sweden 2020

CHALMERS
UNIVERSITY OF TECHNOLOGY

Surface integrity analysis before and after machining of additively manufactured (3D printed) 316L stainless steel using selective laser melting (SLM) and electron beam melting (EBM)

AMIR REZA SHAHAB

Department of Industrial and Materials Science

Chalmers University of Technology

Abstract:

This master thesis work was aimed for understanding the surface integrity and machinability of 316L stainless steel which was produced by two common methods of additive manufacturing called selective laser melting (SLM) and electron beam melting (EBM). Additive manufacturing is a new method of production for complex shape structures with less lead time and less waste of material. Samples of SLM were produced at RISE AB with SLM Solutions machine and samples of EBM were produced at Mid-Sweden university with ARCAM machine. The results of as-printed condition show that melt pools in EBM samples are larger that SLM ones. SLM samples have a cellular structure inside each melt pool. SLM samples have higher hardness than EBM however the surface roughness of SLM samples are lower than EBM. Lack of fusion features in EBM samples are in the size of less than one micron. Samples were machined (turning) from top and bottom in four steps. Depth of cut for each step is 0.25 mm. During turning, all 3 forces of cutting, feed and passive forces were recorded. All components of forces in step 1 are higher in SLM in comparison with EBM. Surface roughness after machining is around 0.9 micron for EBM and 0.8 micron for SLM. It is recommended to machine SLM samples for 1 passage with depth of cut of 0.25 mm. For EBM samples, it is recommended to machine the samples for 3 passages with depth of cut of 0.75 mm. Tensile residual stress exists after additive manufacturing due to rapid solidification of new layer in contact with an already solid layer. Machining will cause compressive stress which neutralizes the tensile stress to some extent. Maximum compressive stress will happen at depth of 10-30 micron under machined surface. In SLM, maximum compressive stress is higher in step1 in comparison with step 4. In EBM, maximum compressive stress is higher in step 4 in comparison with step 1.

Keywords: Additive manufacturing- SLM- EBM- Surface integrity- 316L stainless steel- Machining- Turning- Surface roughness- Residual stress- Microstructure

CHALMERS
UNIVERSITY OF TECHNOLOGY

Acknowledgements

This master thesis work was a one academic year journey from September 2019 until June 2020. Firstly, I would like to thank my parents, Nasrin and Valiollah, for their never-ending support and encouragement. Then I thank Seyed Hosseini, Uta Klement and Dinesh Mallipeddi for their help and support during the thesis. I would like to thank every colleague or employee at RISE AB and Chalmers University that I had interaction with. Finally, I would like to dedicate my work to Arezou for listening to me and supporting me with her nice words.

The thesis work was performed in a collaboration between Chalmers University (CAM2 Center for Additive Manufacturing) and RISE AB Research Institute of Sweden.

AMIR REZA SHAHAB, Gothenburg, June 2020

CHALMERS
UNIVERSITY OF TECHNOLOGY

Table of Contents

Introduction:

In recent years, additive manufacturing has become a trending technology to produce complex shape products with less lead time and less waste of material. 316L is an austenitic stainless steel which is widely used in industry where the corrosion resistance and reasonable mechanical properties are required. Two important techniques of AM are SLM (Selective Laser Melting) and Electron Beam Melting (EBM) for metals. The samples produced with both techniques are near net shape, however the surface quality after production is not good enough for some industrial applications. Therefore, in order to have an acceptable surface quality, a hybrid method is exploited which is a combination of additive manufacturing and machining. The average roughness (Ra) of a sample produced by EBM is about 60 microns, while it is around 6 microns for SLM. Therefore, 1-2 passes of machining are needed to achieve a good surface quality for specific applications.

In the literature, there is limited information regarding machining after additive manufacturing of 316L [1,2]. It is worth mentioning that a heat treatment is sometimes necessary after AM as a post-processing treatment in order to avoid distortion or buckling of the samples and achieving a desirable microstructure [3, 4], however in our case there was no necessity for heat treatment. In this thesis, it is planned to understand the microstructure (OM, SEM, EDX), hardness and roughness of the additively manufactured 316L stainless steel produced by SLM and EBM in as-printed condition and after machining (turning). The machining parameters were selected based on recommendations for Sandvik turning inserts used for conventional machining of stainless steel. Machining forces (cut force, feed force, passive force) were measured online from the turning machine. Afterward the roughness of machined surfaces was measured and compared for SLM and EBM. Finally, residual stress of machined surfaces was measured with XRD technique.

Materials and experimental procedure:

The powder of 316L for SLM was provided by Höganäs AB (Höganäs, Sweden) with average particle size of 15-45 microns and the powder for EBM was provided by Carpenter Powder Products AB (Torshälla, Sweden) with particle size distribution ranging from 53-150 microns. The chemical composition of both powders is shown in tables 1 and 2.

Table 1: Chemical composition of EBM powder

Cr	Ni	Mn	Mo	Si	Fe
18.1	11.2	1.6	1.5	1.0	66.6

Table 2: Chemical composition of SLM powder

Cr	Ni	Mn	Mo	Si	Fe
17.8	13.8	1.5	2.7	0.1	64.1

The 3D printing by laser powder bed fusion is performed in a SLM-125 from SLM Solutions (Germany), and for EBM, an ARCAM EBM A2X from GE Additive ARCAM (Sweden). The machines are shown in figure 1.

Figure 1: SLM printing machine (left) and EBM printing machine (right).

The laser diameter is about 80 microns with power of 200 W and the production is performed under argon gas flow atmosphere. The layer thickness is 30 micron and energy density value is 69 j/mm3. The electron beam diameter is about 180 microns and the production is performed under vacuum. The layer thickness in EBM is between 100 to 200 microns. The samples are cylinders with a length of 110 mm, diameter of 55 mm, and wall thickness of 17.5 mm as shown in figure 2. SLM samples have 2 border lines at the outer surface (90 microns distance) which were scanned before the hatching of core production starts, and the number of borders for EBM samples are 3. Before start of printing, the power in SLM were pre-heated to 200 ºC and in EBM to 800 ºC. The printing pattern and number of borders for each method will be discussed later.

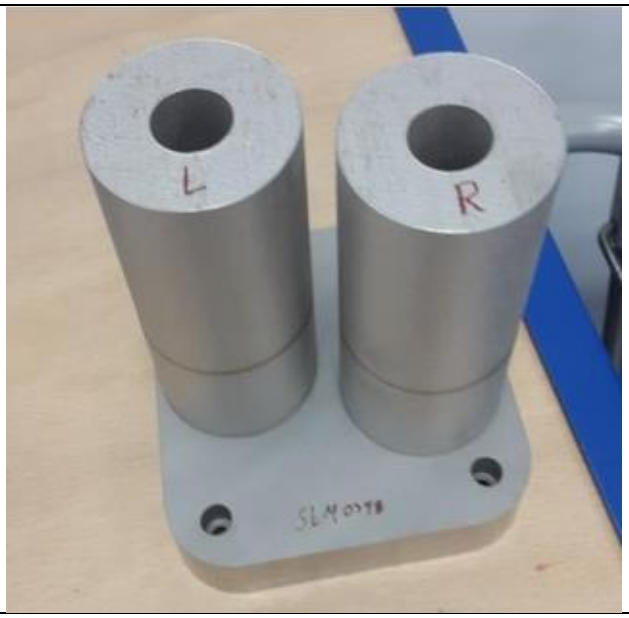

Figure 2: Image of samples produced by SLM.

For revealing the microstructure, samples were prepared according to Struers guideline. Electro-etching with Oxalic acid (3 V) were used for etching. The metallography was done with a light optical microscope (Leica). For microstructural characterization, a Scanning Electron Microscope (SEM) with field emission gun (Leo Gemini 1550 SEM) was used. Chemical analysis was performed with energy-dispersive X-ray spectroscopy (EDX) and a respective detector mounted on the SEM. Microhardness measurements were performed with automatic hardness measurement equipment. Roughness measurements were performed using Sensofar optical profilometer instrument. Residual stress measurements were performed with Stresstech X-ray robotic system.

Results and discussion:

Microstructure: optical and scanning electron microscope

Schematic of sample selection for analysis is shown in figure 3. Sections of top and bottom were selected to study the as-print condition for both SLM and EBM. The surface and center of each section were studied under optical and scanning electron microscope and compared with each other.

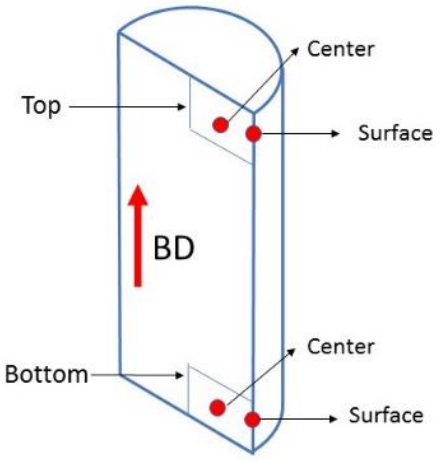

Figure 3: Schematic of sample selection for microstructure analysis.

SLM microstructure at surface of sample from both top and bottom are shown in figures 4 and 5, respectively. In SLM, the surface border layer seems to be about 90 microns in thickness in both top and bottom surface. This matches with the contour and hatch printing pattern.

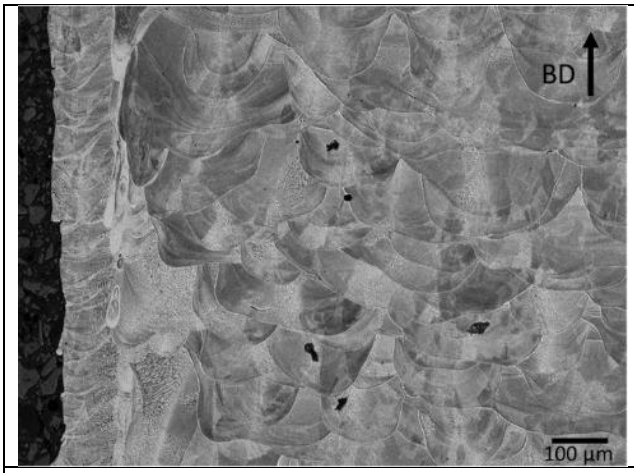

Figure 4: Microstructure of top view for SLM-surface.

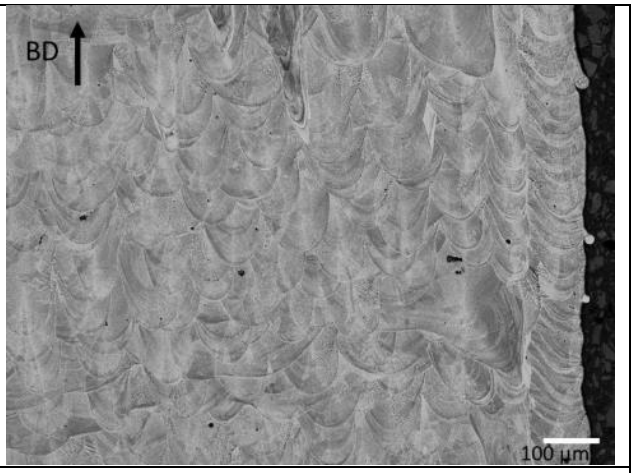

Figure 5: Microstructure of bottom view of SLM-surface.

The schematic of the printing pattern for SLM is shown in figure 6. There are 2 borders and one filling contour for the start of printing, but the hatching will overlap with the filling contour and the 2nd border. Therefore, in the microstructure images, it is only possible to recognize the 1st border that extends about 90 microns from the surface.

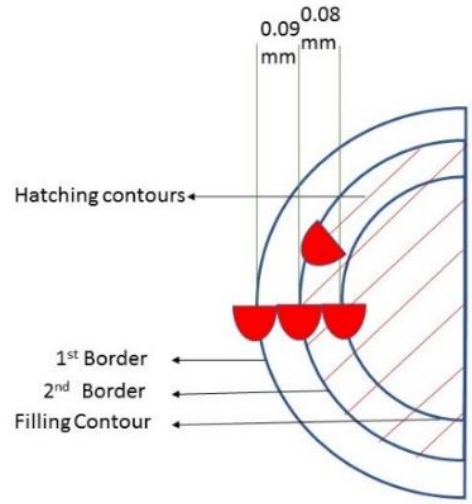

Figure 6: Printing pattern for SLM samples.

Melt pool diameters at the top and bottom surfaces are different in size. Melt pools at the top surface are about 130 microns in diameter and at the bottom surface they are around 80 microns.

Some melt pools at top surface overlapped with each other. It seems the overlapping of melt pools in other direction comes from the 67 degrees rotation for the printing of next layer. Overlapping happens because each new layer will melt the one in the previous layer to some extent during printing of new layer.

Figures 7 and 8 show the microstructures of center part of top and bottom of SLM samples. The difference in melt pool sizes is still visible.

Figure 7: Microstructure of top view for SLM-center.

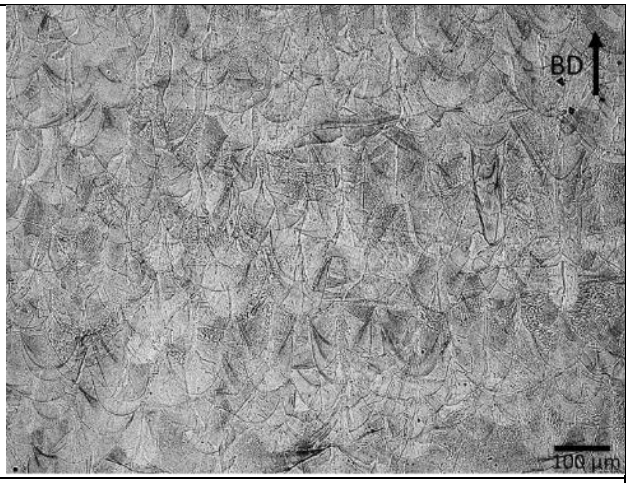

Figure 8: Microstructure of bottom view for SLM-center.

In SLM microstructure, we do not expect any sigma phase or carbides because after melting by laser, the samples quench very rapidly with cooling rate of 10^5-10^7 ºC/sec which is very fast and does not allow the equilibrium phases to form. So, the final structure is almost pure austenite. It is called "hardened austenite" with cellular structure but heat treatment above 1100 ºC will cause precipitation of delta ferrite in the microstructure [5,6].

SEM images of SLM samples are shown in figures 9-14. They show the cellular structure inside each melt pool in figures 13, 14 and the orientation of each zone in comparison to the neighbors in figures 11, 12. The cell size is approximately 0.5-1 micron shown in figure 14. Cell structures have been reported in the literature for SLM [7].

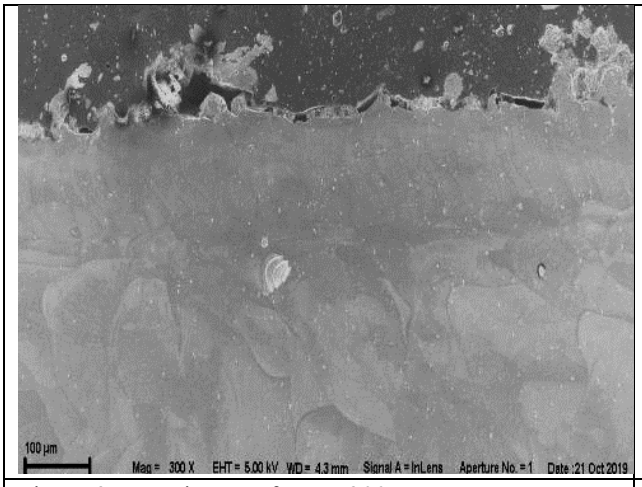

Figure 9: SEM image of SLM-300X.

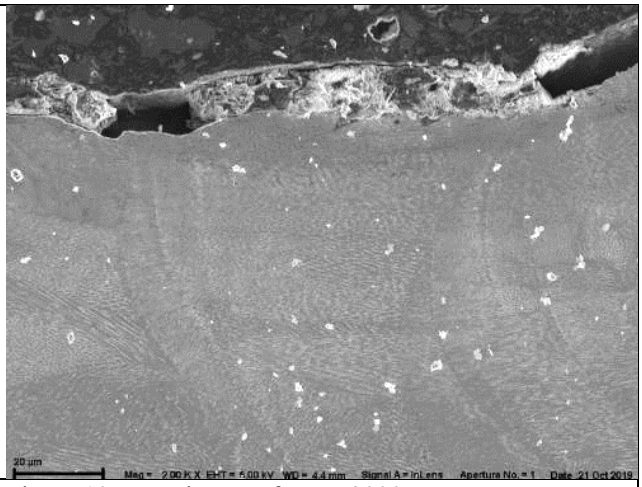

Figure 10: SEM image of SLM-2000X.

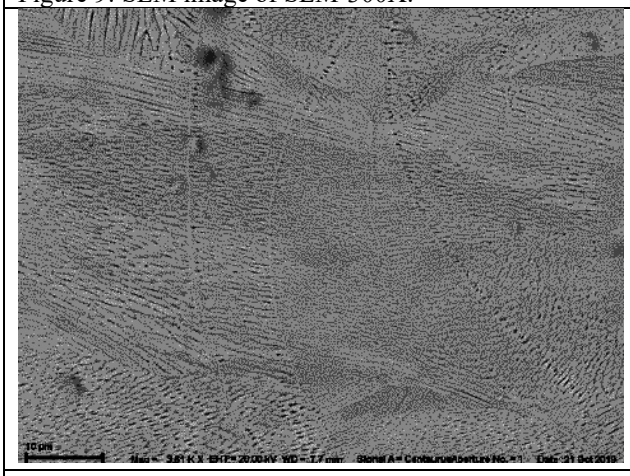

Figure 11: SEM image of SLM-3600X.

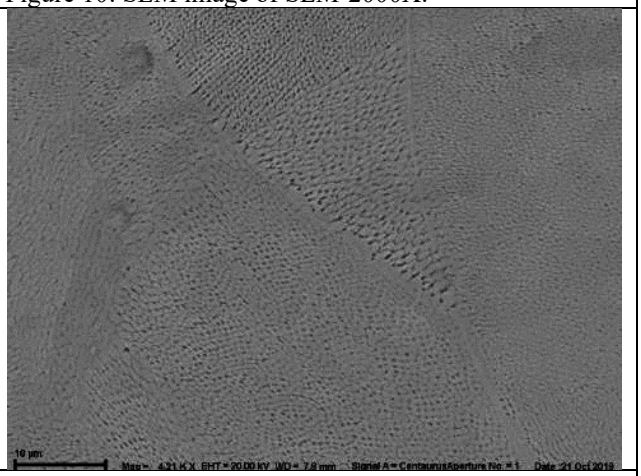

Figure 12: SEM image of SLM-4200X.

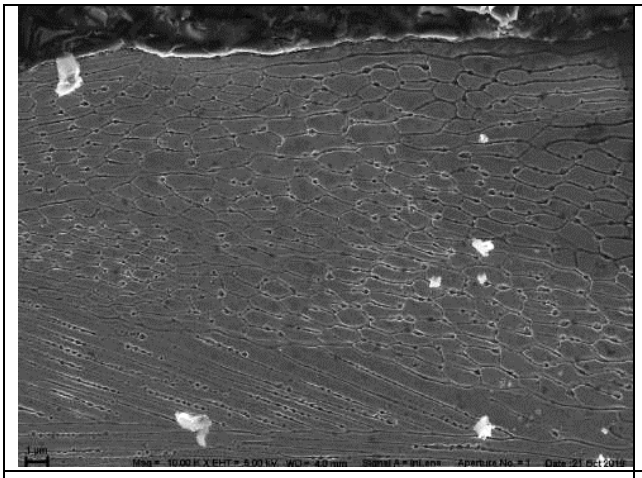

Figure 13: SEM image of SLM-10000X.

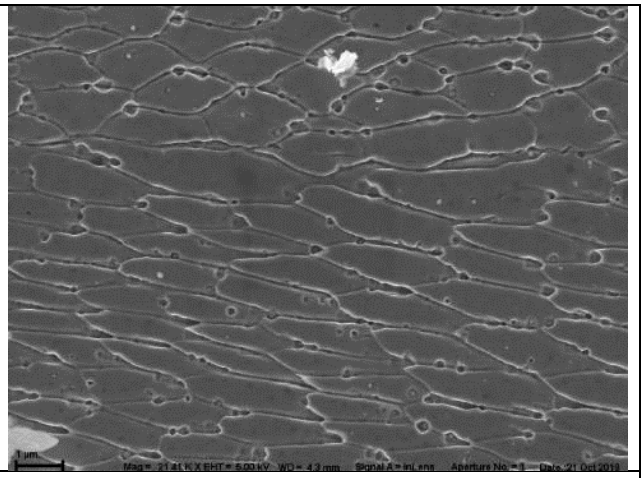

Figure 14: SEM image of SLM-21000X.

The microstructure of top and bottom surfaces of EBM samples are shown in figures 15 and 16. The outer surface includes 3 layers at top and bottom. Each layer contains melt pools with the size of about 250 microns. Melt pool diameters seem to be similar at top and bottom surface and are about 250 microns. This is possible because the electron beam diameter can be in range of 110-180 microns. For better view of 3 border layers, the microstructure is shown with lower magnification in figure 17.

The microstructure produced by EBM shows larger melt pools than when using SLM and elongated grains crossing the melt pools which grow in the direction of the thermal gradient. These elongated grains are more prominent at the bottom surface.

Figure 15: Microstructure of top view for EBM-surface.

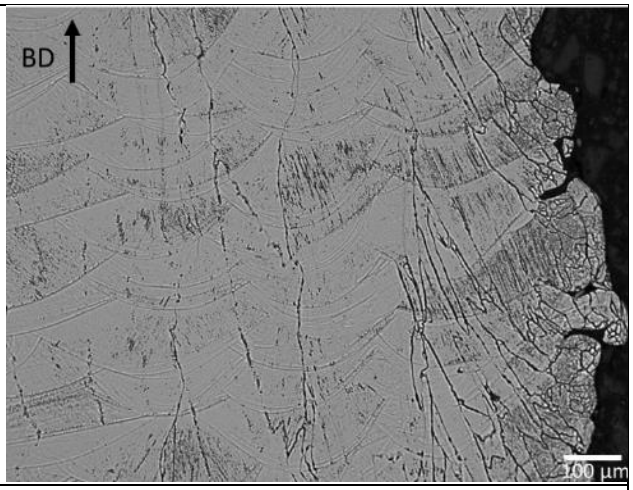

Figure 16: Microstructure of bottom view for EBM-surface.

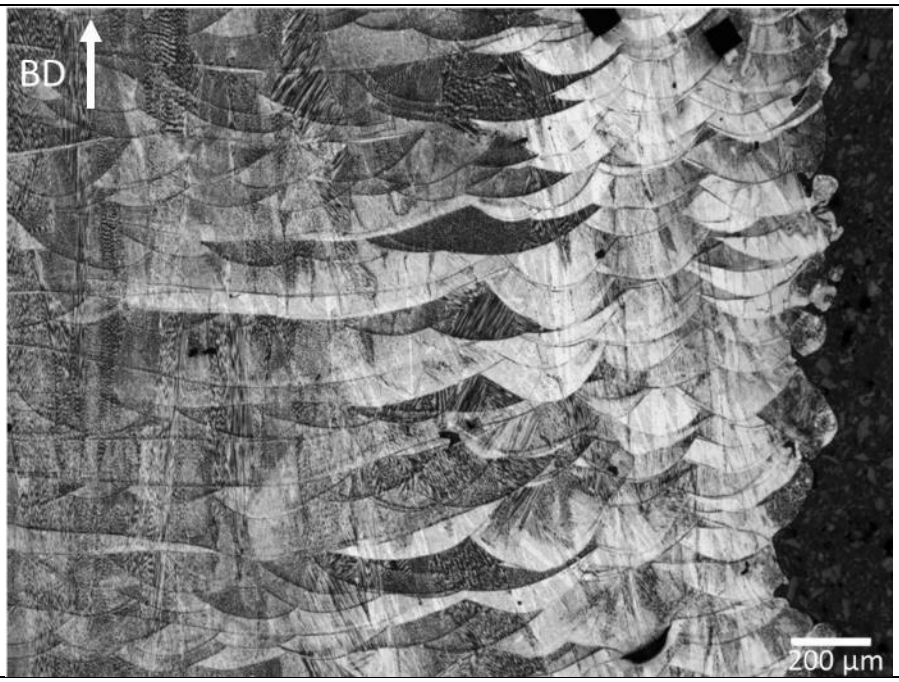

Figure 17: Microstructure of top view for EBM with lower magnification. It is possible to distinguish the 3 borders.

The proposed scanning pattern is shown in figure 18. There are 3 borders which are in distance of about 180 microns from each other and the internal filling contour which will be overlapped by the hatching contours printing. Therefore, it is possible to see 3 borders in the microstructure as shown in figure 17.

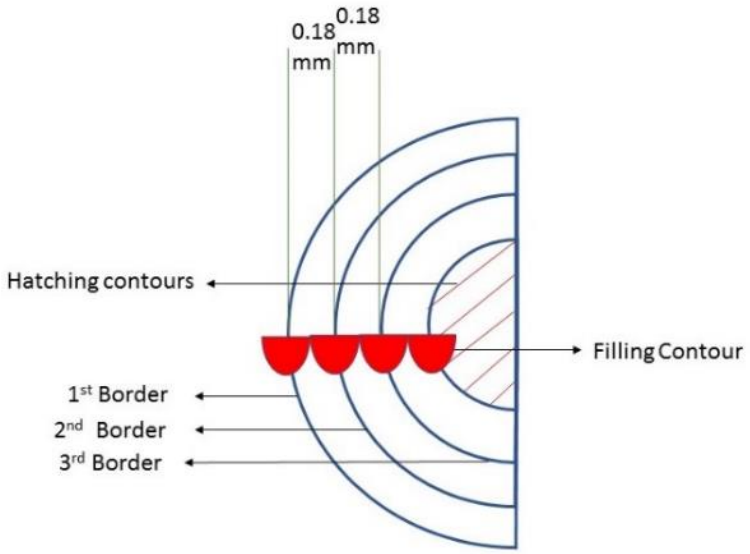

Figure 18: Printing pattern for EBM samples.

Figures 19 and 20 show the microstructure at the center of the top and bottom sections of the EBM sample. Elongated grains are clear and visible in the bottom section. Elongated grains grow in direction of thermal flow in building direction and cross through the melt pools and printing layers.

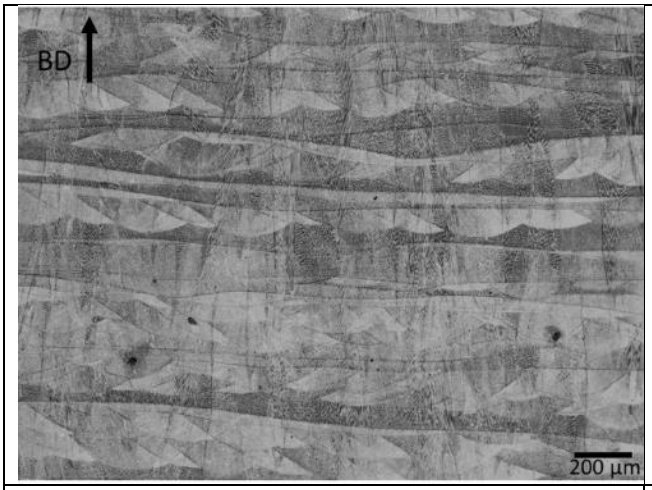

Figure 19: Microstructure of top view for EBM-center.

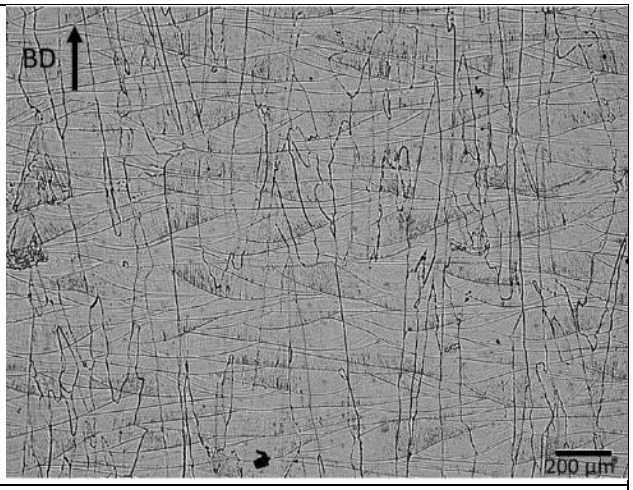

Figure 20: Microstructure of bottom view for EBM-center.

Figure 21 shows the bottom part of the EBM sample at 200X magnification. Melt pools and elongated grains are clearly visible in the image. As can be seen, black features are present inside the melt pools and decorate the grain boundaries. In EBM, the powder is pre-heated up to 700-800 ºC before the start of printing. Therefore, it is possible to see some precipitates in EBM sample.

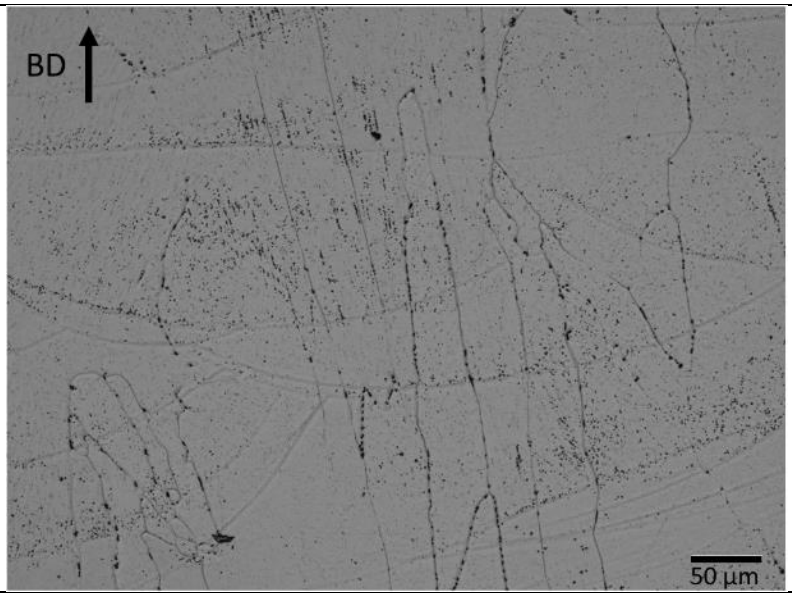

Figure 21: Microstructure of bottom view for EBM with higher magnification.

SEM images of EBM samples are shown in figures 22-26. They do not show cellular structure, but they clearly show some features inside the melt pools and along the boundaries of elongated grains. The features have the size of a few microns however we will call them as features since it is not clear whether they are precipitates or lack of fusion. The chemical analysis of these features will be performed later by EDX analysis.

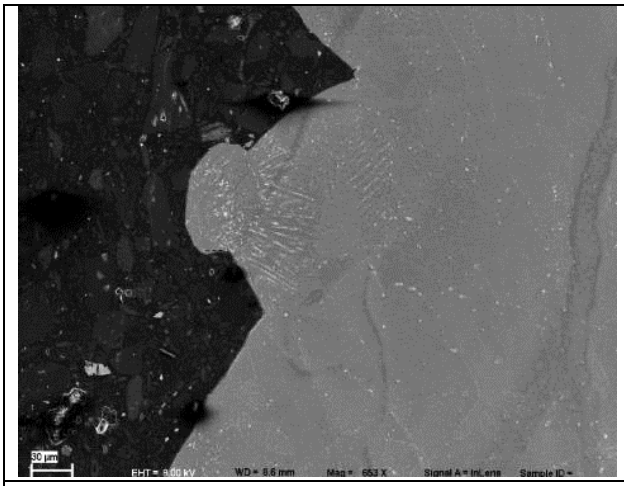

Figure 22: SEM image of EBM.

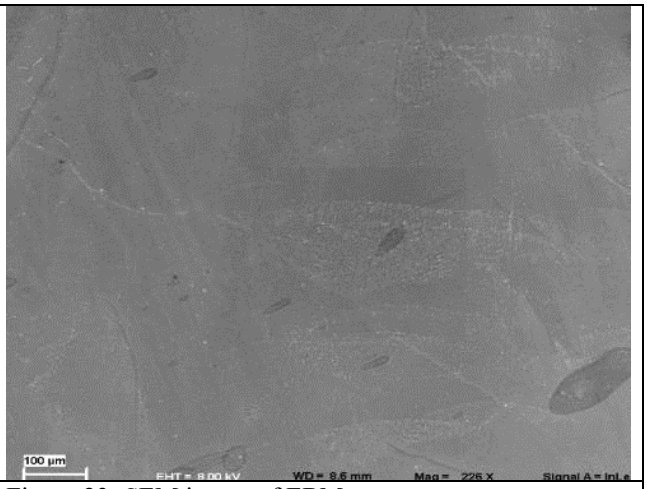

Figure 23: SEM image of EBM.

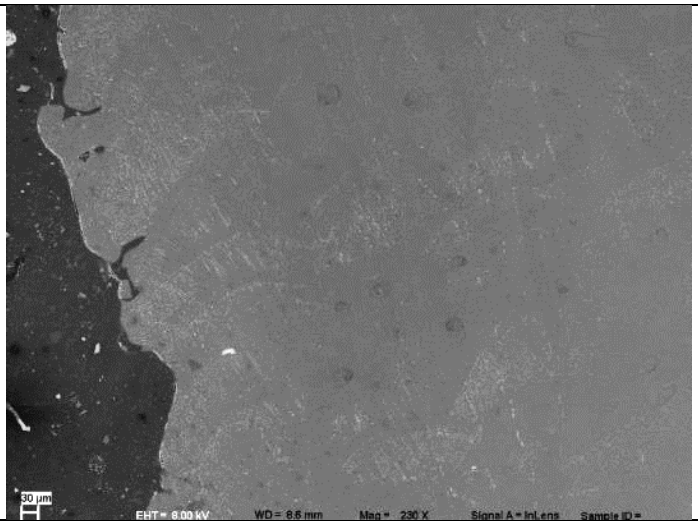

Figure 24: SEM image of EBM. Melt pool boundaries are clear.

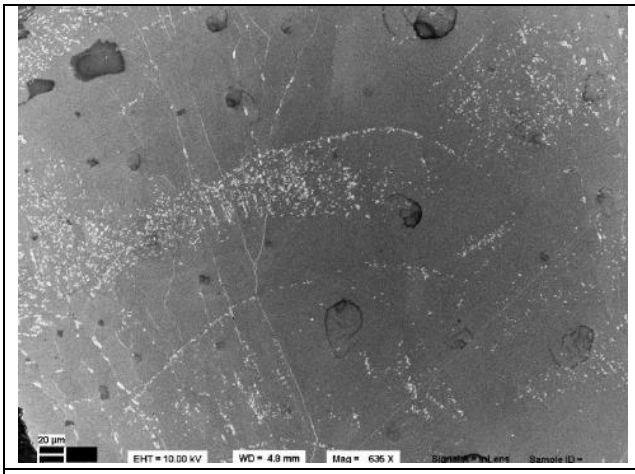

Figure 25: SEM image of EBM.

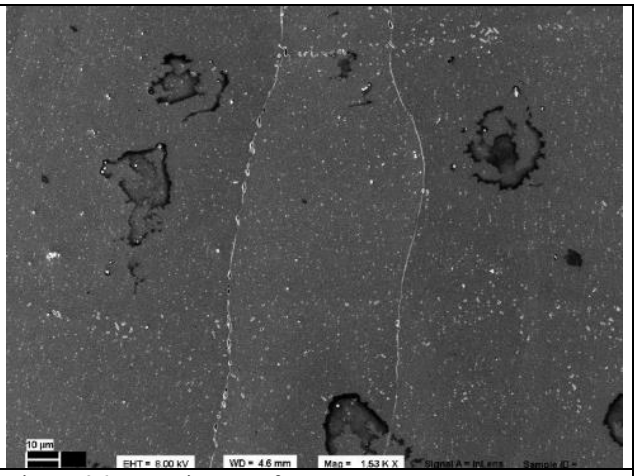

Figure 26: SEM image of EBM.

Surface roughness

Figures 27 and 28 show the microstructure at the surface of the SLM sample as well as the corresponding 3D surface roughness profile. Surface roughness is measured according to standard ISO 25178 over the surface area of 4.0 x 0.6 mm.

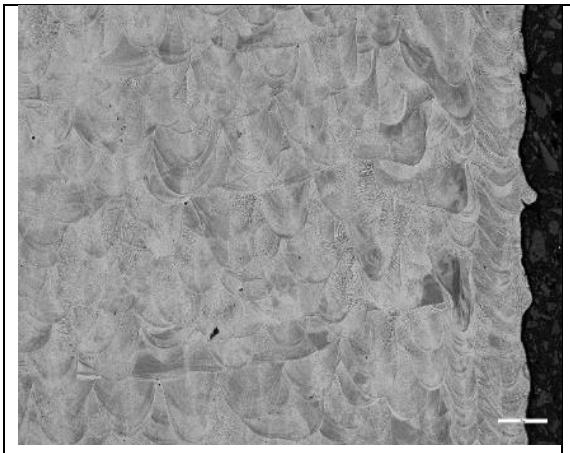

Figure 27: Typical microstructure of SLM sample.

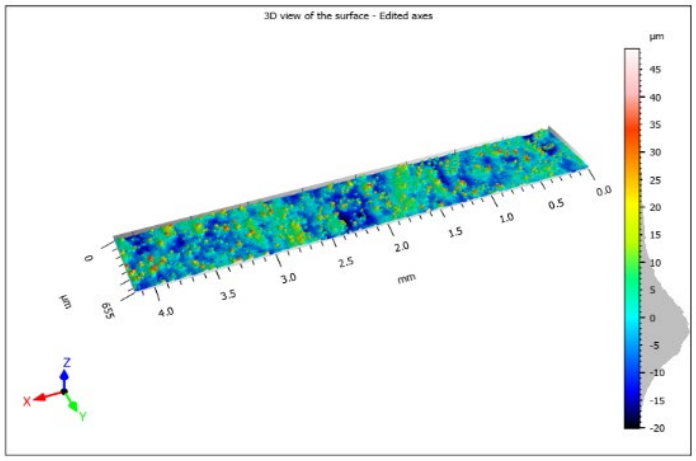

Figure 28: SLM surface roughness profile.

Figures 29 and 30 show the microstructure at surface of the EBM sample and the corresponding 3D surface roughness profile.

Figure 29: Typical microstructure of EBM sample.

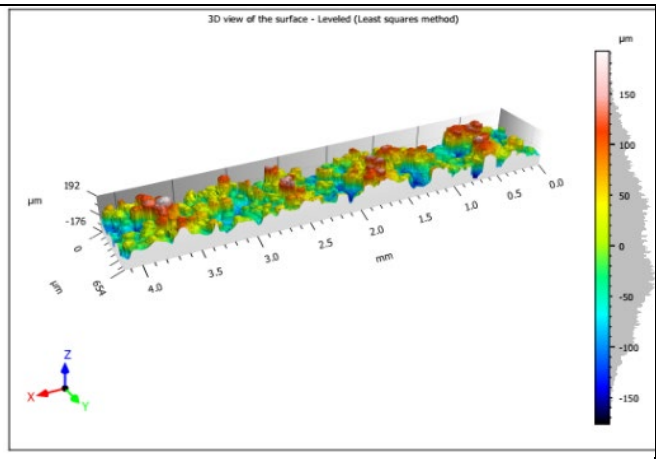

Figure 30: EBM surface roughness profile.

The results of surface roughness measurements are shown in table 3. As can be seen, the average surface roughness (Sa) of the EBM samples are about 9 times higher than for the SLM samples. The difference can be directly observed in figures 27 and 29. The magnification of both images are the same. The protrusions in EBM is much larger than in SLM, therefore the surface roughness of EBM is higher.

Table 3: Roughness measurement values for SLM and EBM

ISO 25178	SLM	EBM
Sa-Arithmetic mean height (micron)	6	55
Sq-Root mean square height (micron)	8	66
S10z-10 point height (micron)	55	400

Overall surface roughness profiles are shown in figures 31 and 32 for better understanding.

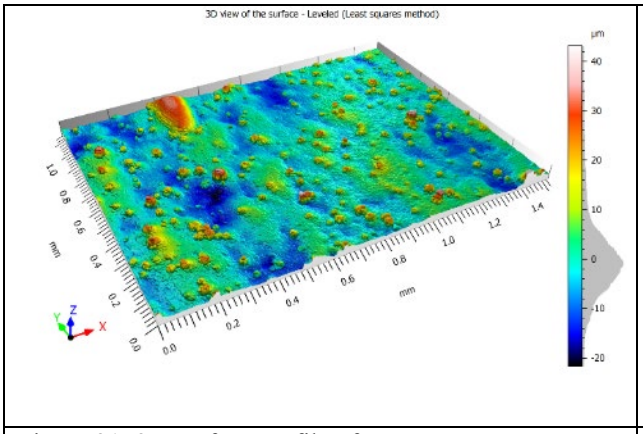

Figure 31: 3D surface profile of SLM.

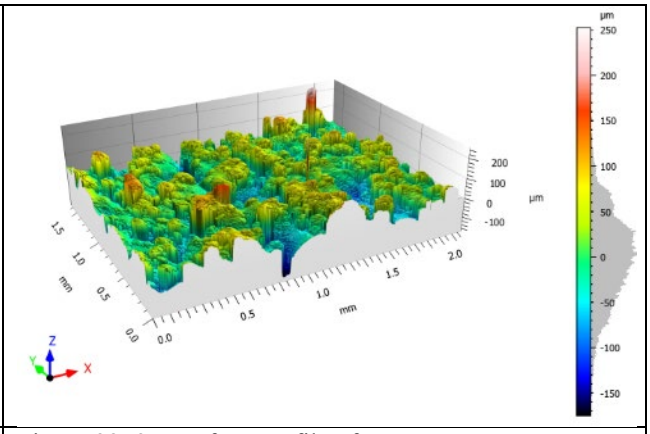

Figure 32: 3D surface profile of EBM.

Microhardness

Microhardness is measured with 0.1 Kg force and 10 sec dwell time. Hardness measurements are performed from the outer surface up to about 1 mm toward the core with interval of 87 microns. This distance is chosen because the indentation diameter is about 35 microns. Total of 12 different distances from the surface are measured and for each distance, 5 indents have been applied and the average of the values are reported including standard deviation. The hardness profiles of top and bottom for SLM and EBM samples are shown in figure 33.

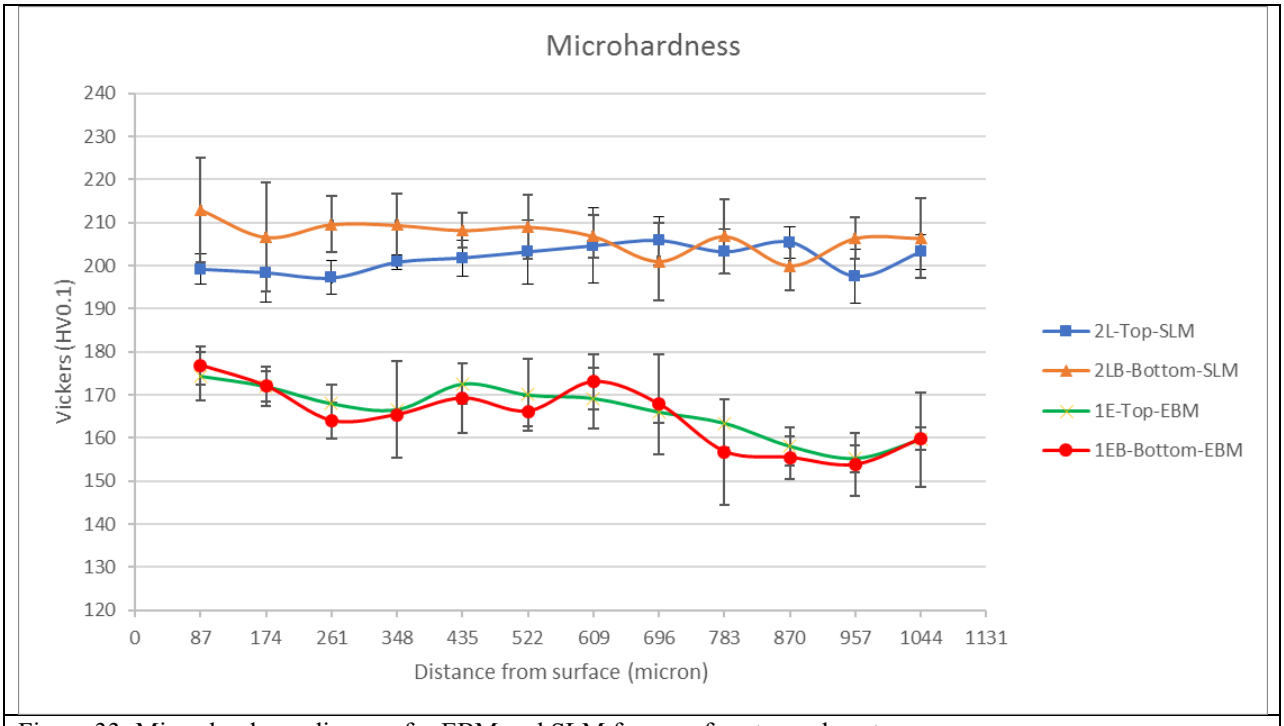

Figure 33: Micro-hardness diagram for EBM and SLM from surface toward center.

As a general trend, the hardness of SLM samples are about 30-40 Vickers higher than EBM samples.

Hardness values in SLM samples vary between 197 and 213 Vickers. In SLM, the bottom layer has higher hardness than the top layer up until about 600 microns from the surface. Afterward, they seem to have the same hardness. In the bottom layer, the hardness decreases when going from surface to center but it is increasing in top layer from surface toward center. The higher hardness of the bottom layer is reported in literature [8] and it is due to the formation of nano-sized oxides like silicon oxide which are more spread at the bottom of SLM components.

In EBM, the hardness varies between 155 and 175 Vickers which is in accordance with what is reported by Rannar et al. [9]. The hardness decreases from the surface toward the center of the component. The hardness profile variations at the top and bottom surface of EBM samples are similar. This can be due to the fact, that all the sample will be kept at a temperature of 800 ºC during production which is called self-annealing in this process [10].

The hardness values of SLM is in accordance with results obtained by Yadollahi et al. [4], i.e. the hardness value is around 200-210 Vickers. In this paper, the hardness value strongly depends on where the indentation is performed. For example, columnar structure has lower hardness than equiaxed structure. The manufacturing method used by Yadollahi et al is direct laser deposition (DED).

Comparatively, the hardness of SLM samples is a bit lower than the values reported in literature. This can be caused by the fact that the powder in this study is heated to around 200 ºC before and during the production. This will coarsen the austenite grains and will lower the hardness.

EDX chemical analysis

SEM images and EDX analysis of 2 different features from EBM samples are shown in figures 34 and 35. The features are around 1 micron in size. EDX analysis shows that there are depletions of Fe, Cr, Ni and Mn in the features however the amounts of Si and Mo remained the same as in the matrix. Depletion of Fe and Ni are reported in literature [11]. There is a possibility that these features are happened due to lack of fusion.

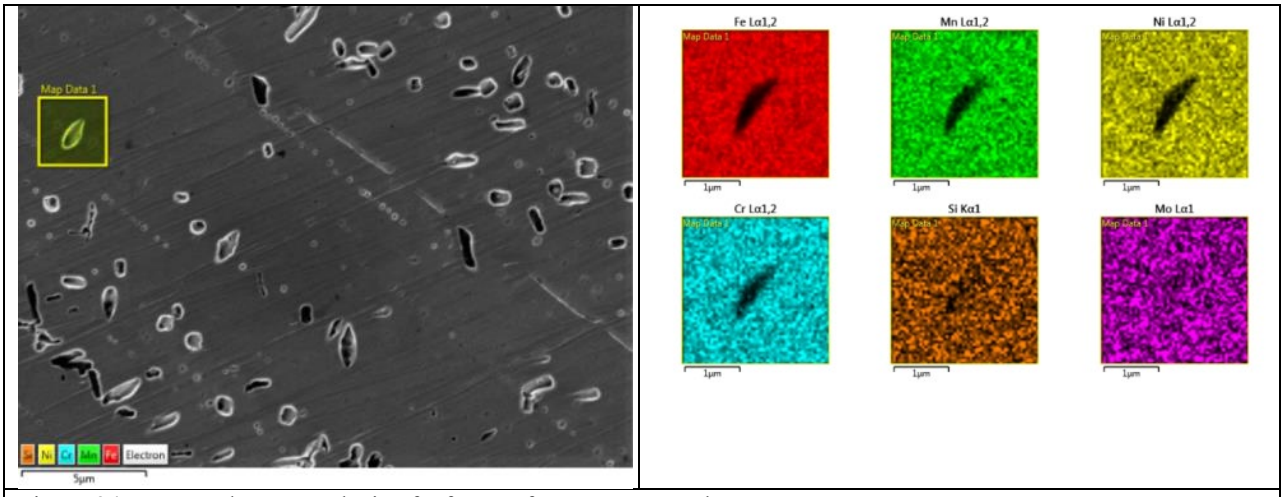

Figure 34: SEM and EDX analysis of a feature from EBM sample.

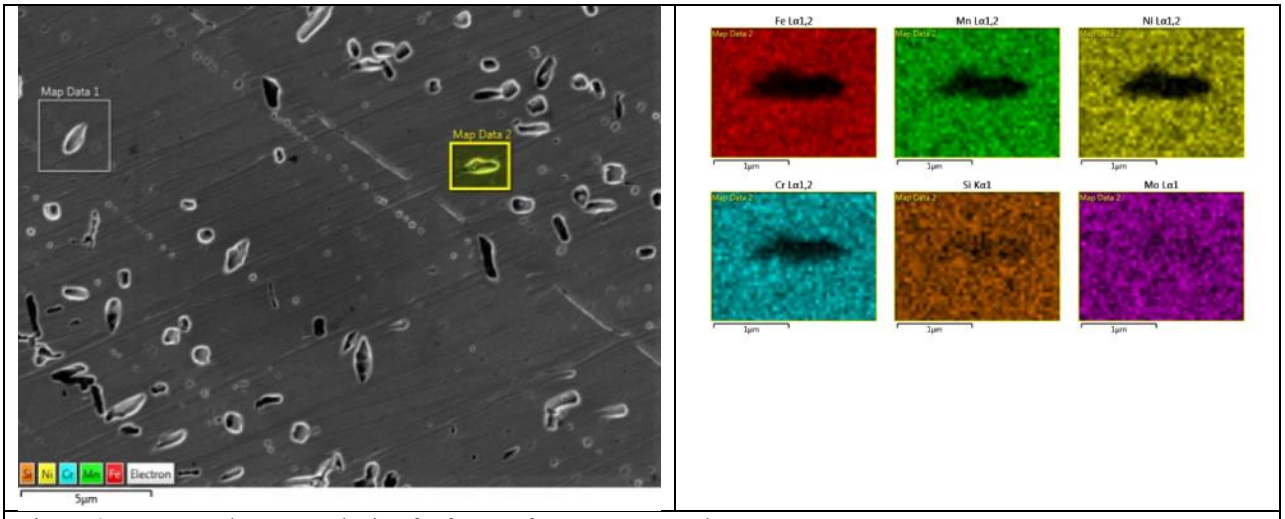

Figure 35: SEM and EDX analysis of a feature from EBM sample.

Machining maps and steps

Turning was selected as the machining method. All the samples were machined from top and bottom. There were 3 samples from EBM and 5 samples from SLM method available for machining. Therefore, a reasonable machining map were designed to cover the most properties. 10 cutting inserts were ordered from Sandvik with designation number of SF 1125. Three different cutting speed of 130, 150 and 230 m/min and three different feed rate of 0.1, 0.15 and 0.2 mm/rev were selected according to the recommendation from Sandvik for the cutting insert. The selected machining map for turning experiments is shown in figure 36.

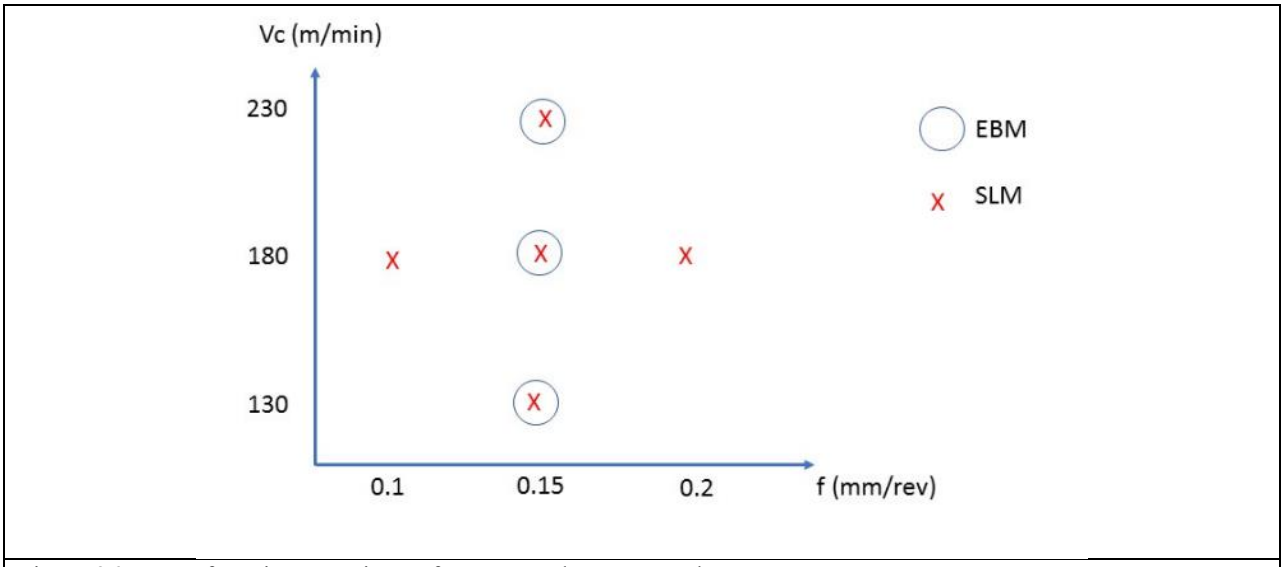

Figure 36: Map of turning experiment for SLM and EBM samples.

The samples were machined from both of top and bottom in 4 steps. Depth of cut is constant for each step with the value of 0.25 mm however it is cumulative for the next steps. It means that depth of cut for step 2 is 0.5 mm, step 3 is 0.75 mm and step 4 is 1 mm. Length of cut for step 1 is 50 mm, step 2 is 40 mm, step 3 is 30 mm and step 4 is 20 mm. Typical machined surfaces for SLM and EBM samples are shown in figures 37, 38.

Figure 37: Typical machined surface and steps for SLM sample.

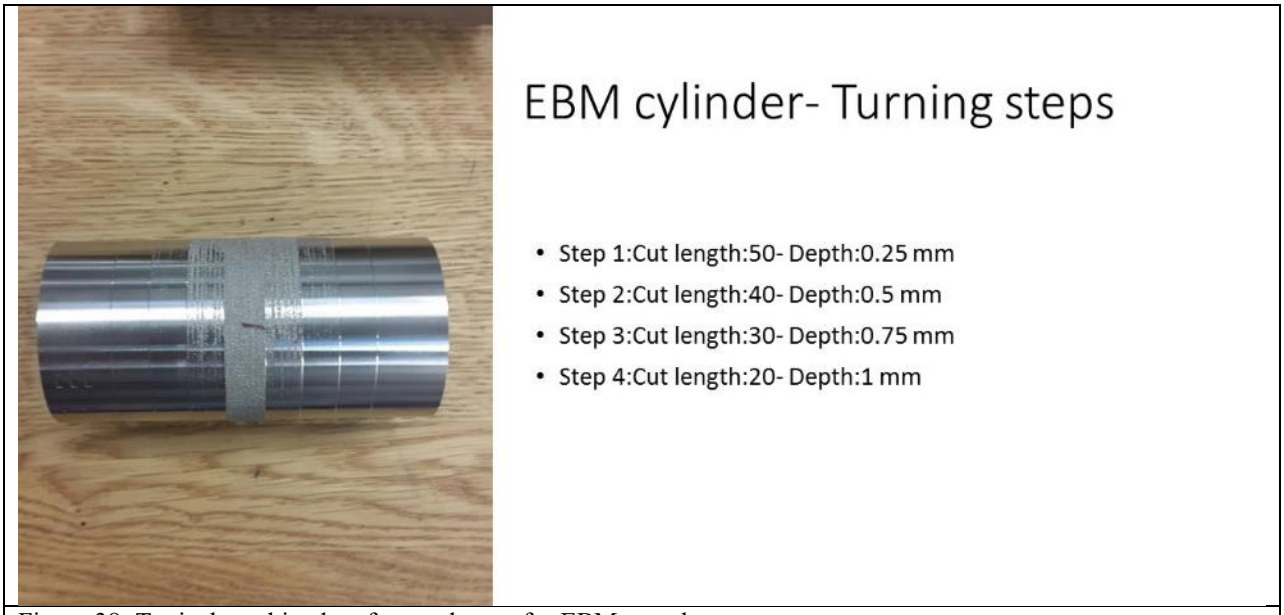

Figure 38: Typical machined surface and steps for EBM sample.

Machining forces

Machining forces were recorded through a data acquisition system which was connected to the turning machine. The set-up of turning machine is shown in figure 39 and the cutting insert SF 1125 from Sandvik is shown in figure 40. Three different components of machining forces are recorded as cutting force, feed force and passive force. Registration of cutting forces during turning are reported in literature [12-14].

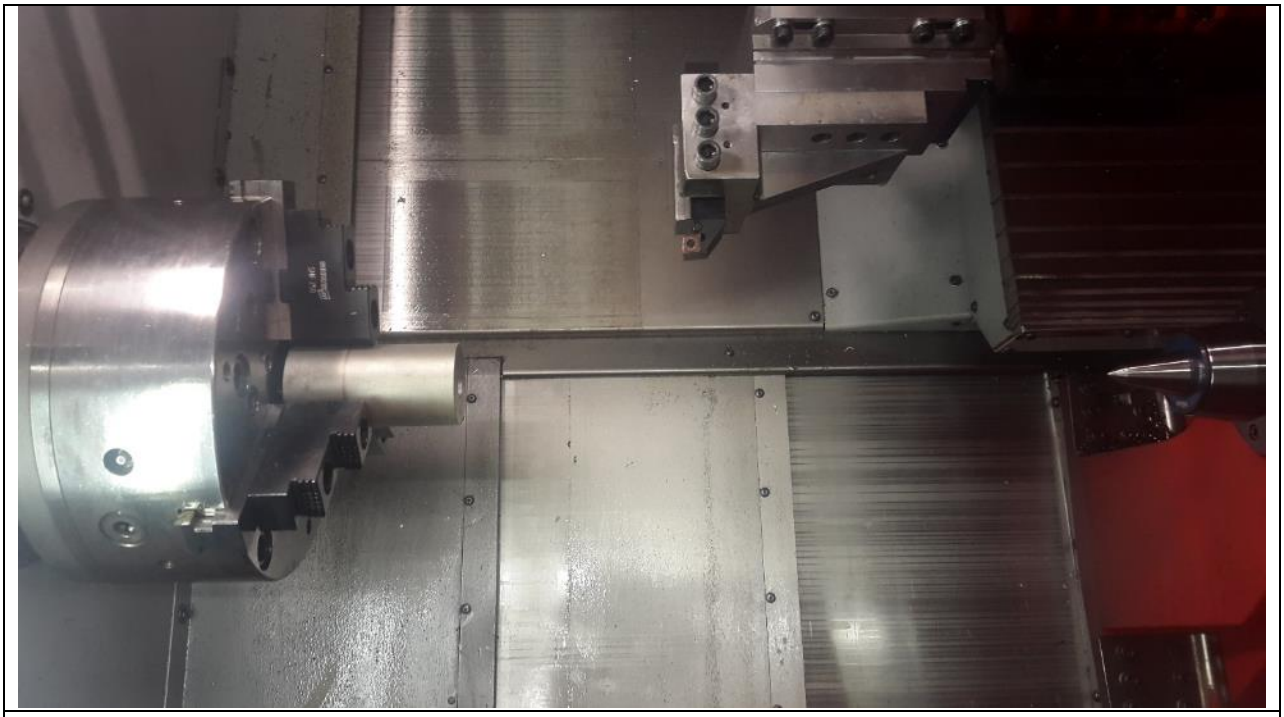

Figure 39: Set up of turning machine.

Figure 40: Cutting insert of SF 1125 from Sandvik.

Cutting force is the components of the force acting on the rake face of the tool which is normal to cutting edge in the direction of motion of workpiece. It is also called tangential force. Feed force is the force component acting on the tool in the direction parallel with the direction of feed.

It is also called as axial force. Passive force is the force that pushes the cutting tool away from the workpiece in radial direction. A schematic of machining forces is shown in figure 41 [13].

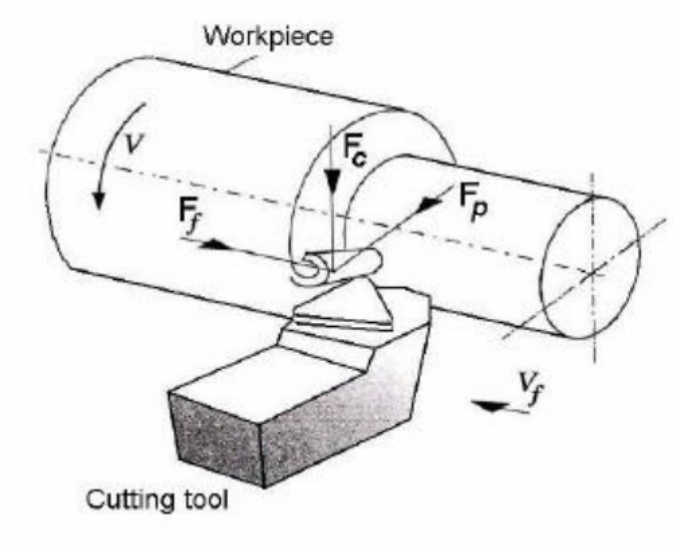

Figure 41: Schematic image of machining forces [13].

For comparison reasons and due to limited number of samples the feed rate was selected to be constant with the value of 0.15 mm/rev but the cutting speeds were different values of 130, 180 and 230 m/min. The selected part of the map is shown in figure 42 by a rectangle.

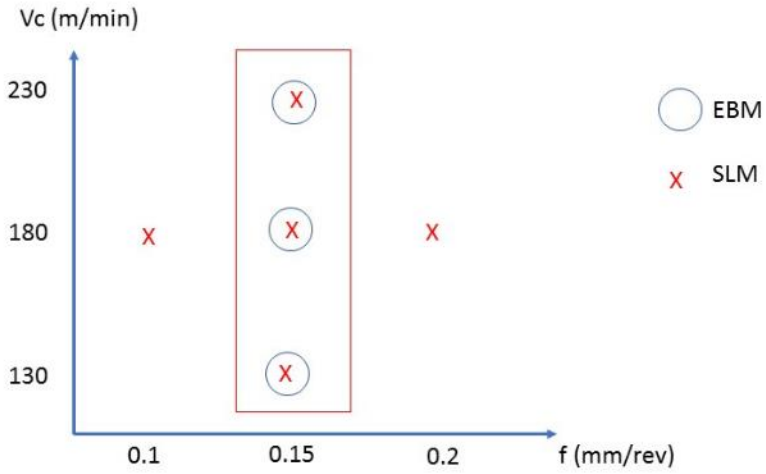

Figure 42: Map of turning experiment for SLM and EBM samples with constant feed rate.

For SLM part the 3 components of forces are shown in figures 43-45.

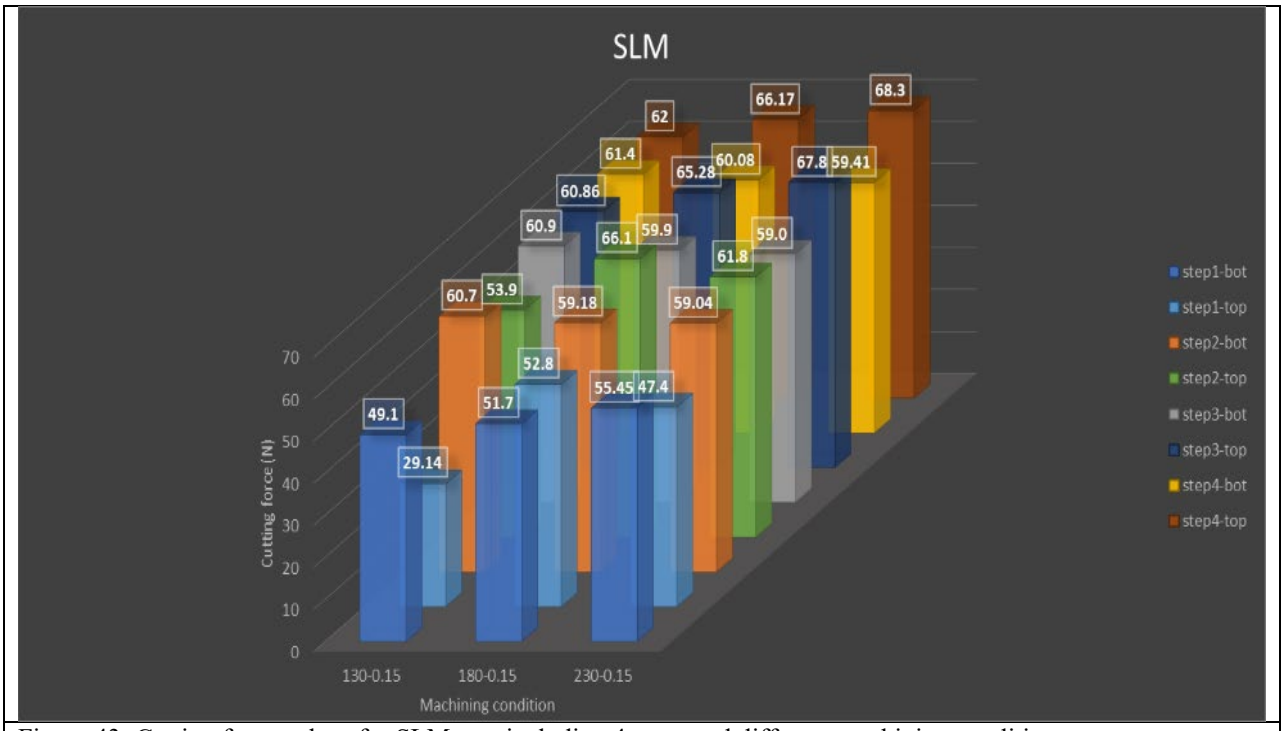

Figure 43: Cutting force values for SLM part including 4 steps and different machining conditions.

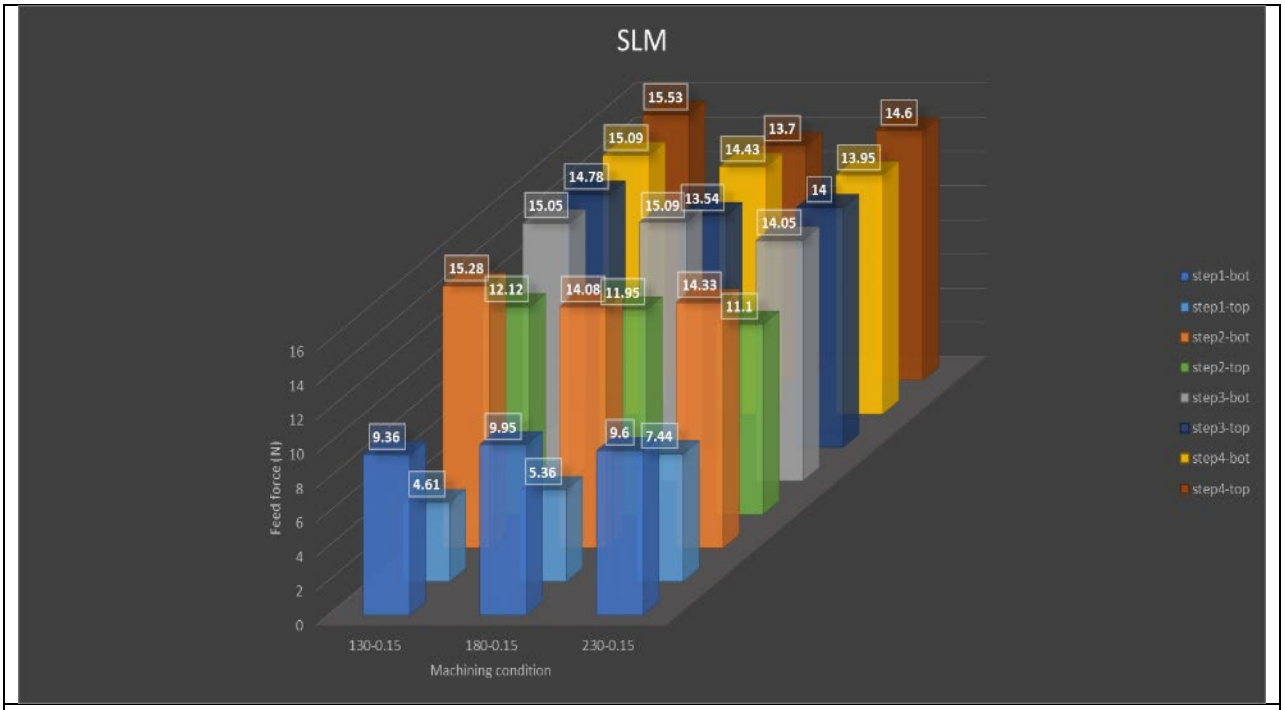

Figure 44: Feed force values for SLM part including 4 steps and different machining conditions.

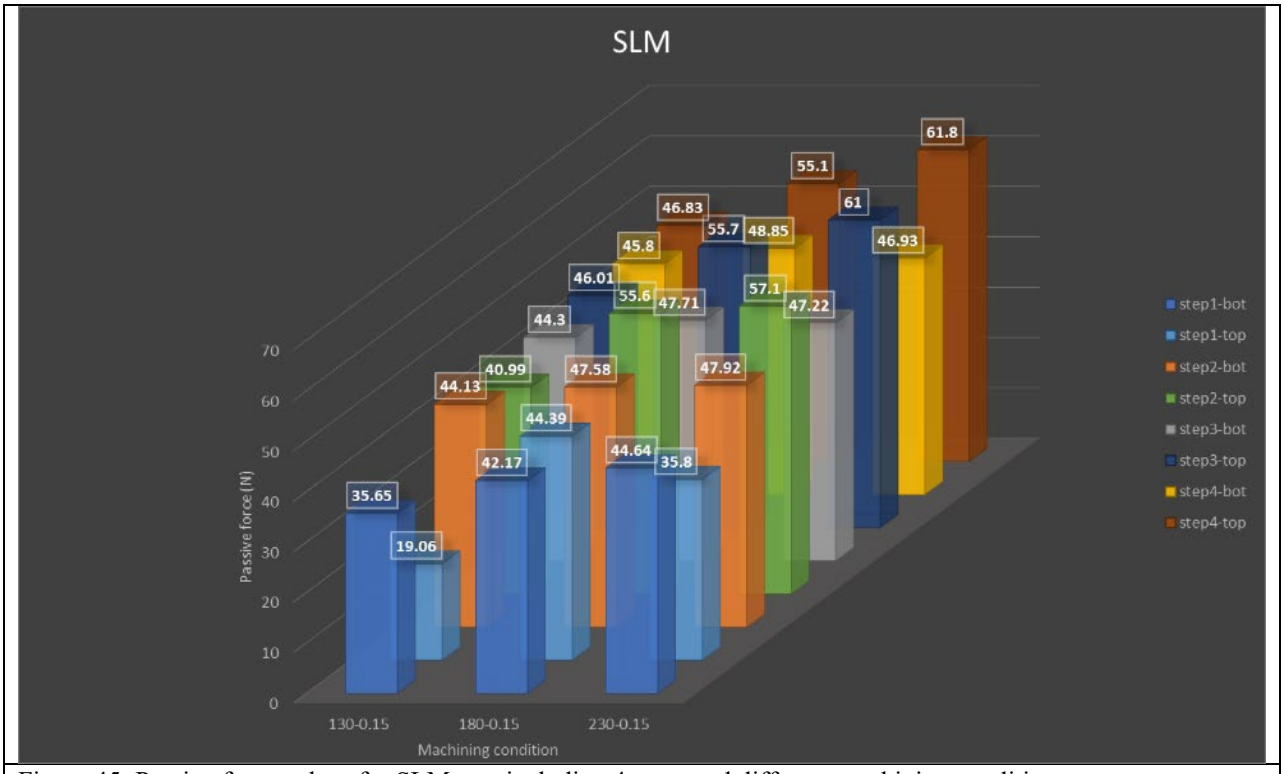

Figure 45: Passive force values for SLM part including 4 steps and different machining conditions.

At the bottom, all 3 components of forces in step 1 are lower than in other steps but it reaches a plateau in steps 2,3 and 4. However, the force values in step 1 increases by increasing the cutting speed from 130 to 230 m/min.

At the top, the cutting force values in steps 1 and 2 increases by moving from 130 to 180 m/min but then decreases by moving from 180 to 230 m/min. However, the cutting force values in steps 3 and 4 increases by moving from 130 to 230 m/min.

For EBM part the 3 components of forces are shown in figures 46- 48.

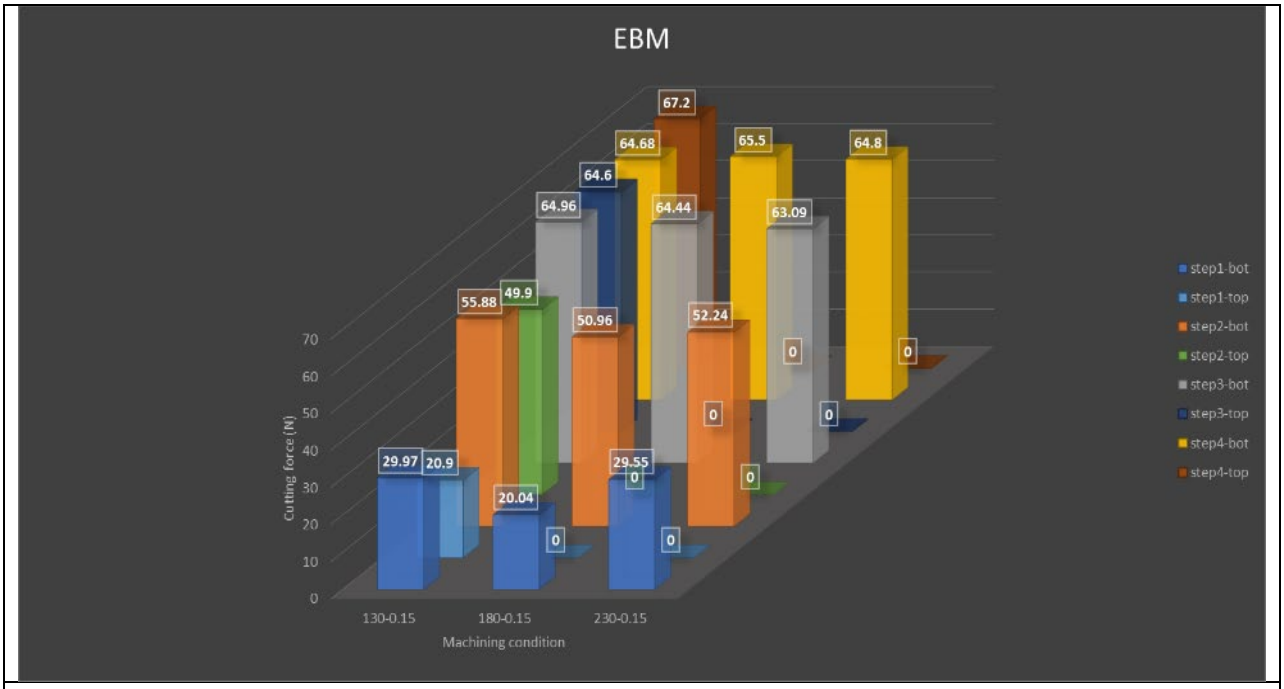

Figure 46: Cutting force values for EBM part including 4 steps and different machining conditions.

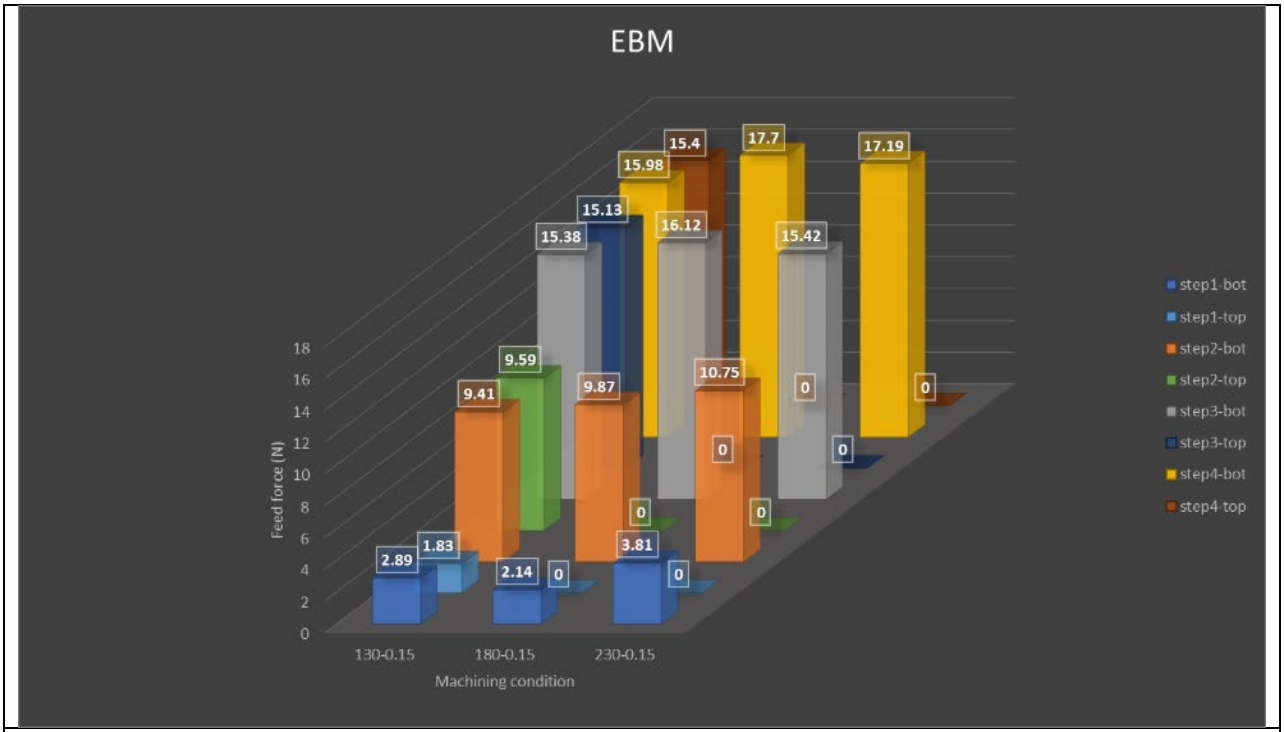

Figure 47: Feed force values for EBM part including 4 steps and different machining conditions.

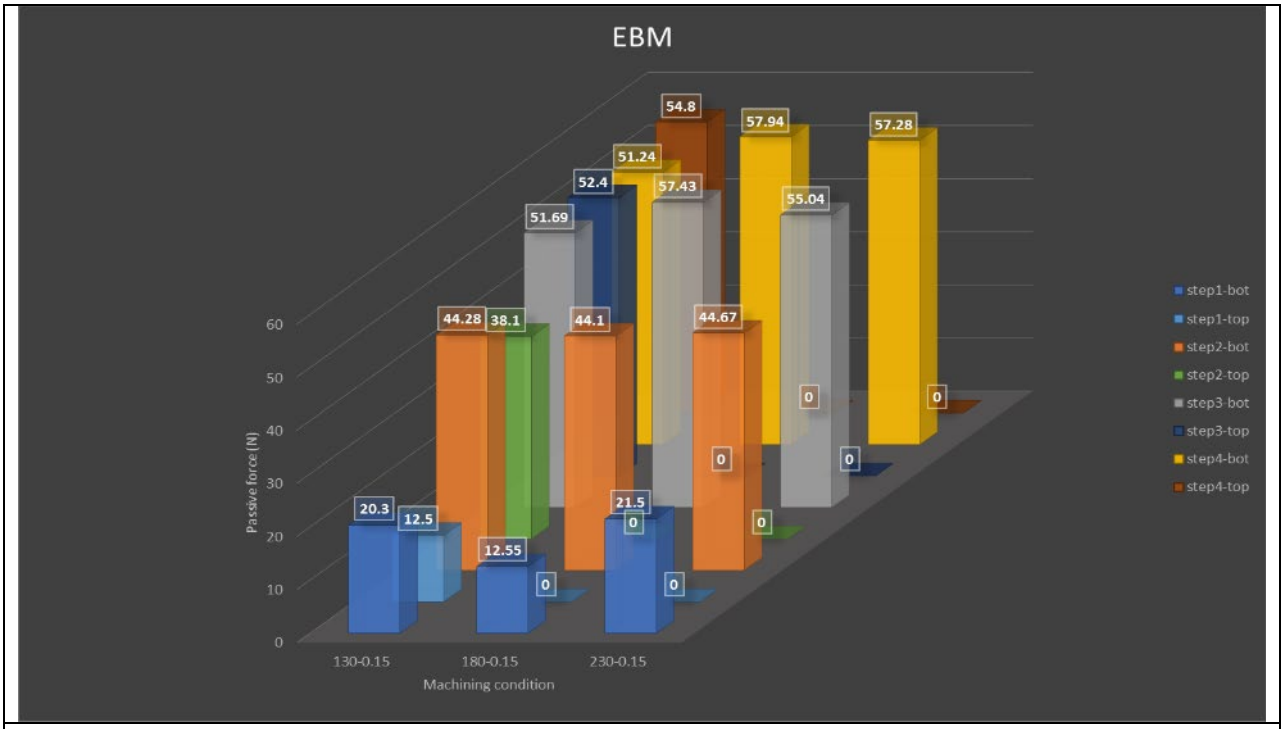

Figure 48: Passive force values for EBM part including 4 steps and different machining conditions.

At the bottom, the cutting forces in step 1 and 2 decreases by moving from 130 to 180 m/min but increases by moving from 180 to 230 m/min. The cutting forces for step 3 and 4 remain constant for all of the cutting speeds. The feed force in step 1 decreases by moving from 130 to 180 m/min but increases by moving from 180 to 230 m/min. The feed forces in step 3 and 4 increases by moving from 130 to 180 m/min however they decrease by moving from 180 to 230 m/min. The passive force in step 1 decreases by moving from 130 to 180 m/min but increases by moving from 180 to 230 m/min. The passive forces in step 2 remains almost constant for all the cutting speeds.

At the top, an error occurred, and the forces were recorded just in cutting speed of 130 m/min. As it can be seen, all the components of forces (cutting, feed, passive) increase from step 1 up to step 4 at the cutting speed of 130 m/min.

For comparison of SLM samples with constant cutting speed of 180 m/min the feed force varied from 0.1 to 0.15 and 0.2 mm/rev. The selected map is shown with a rectangle in figure 49.

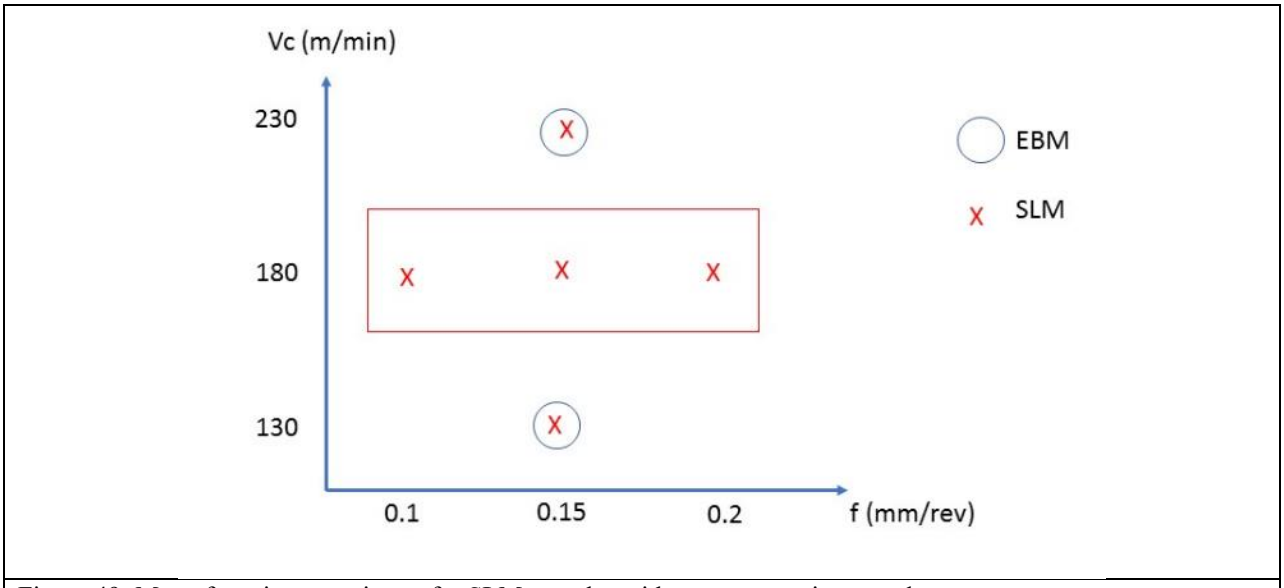

Figure 49: Map of turning experiment for SLM samples with constant cutting speed.

For SLM part the 3 components of forces are shown in figures 50-52.

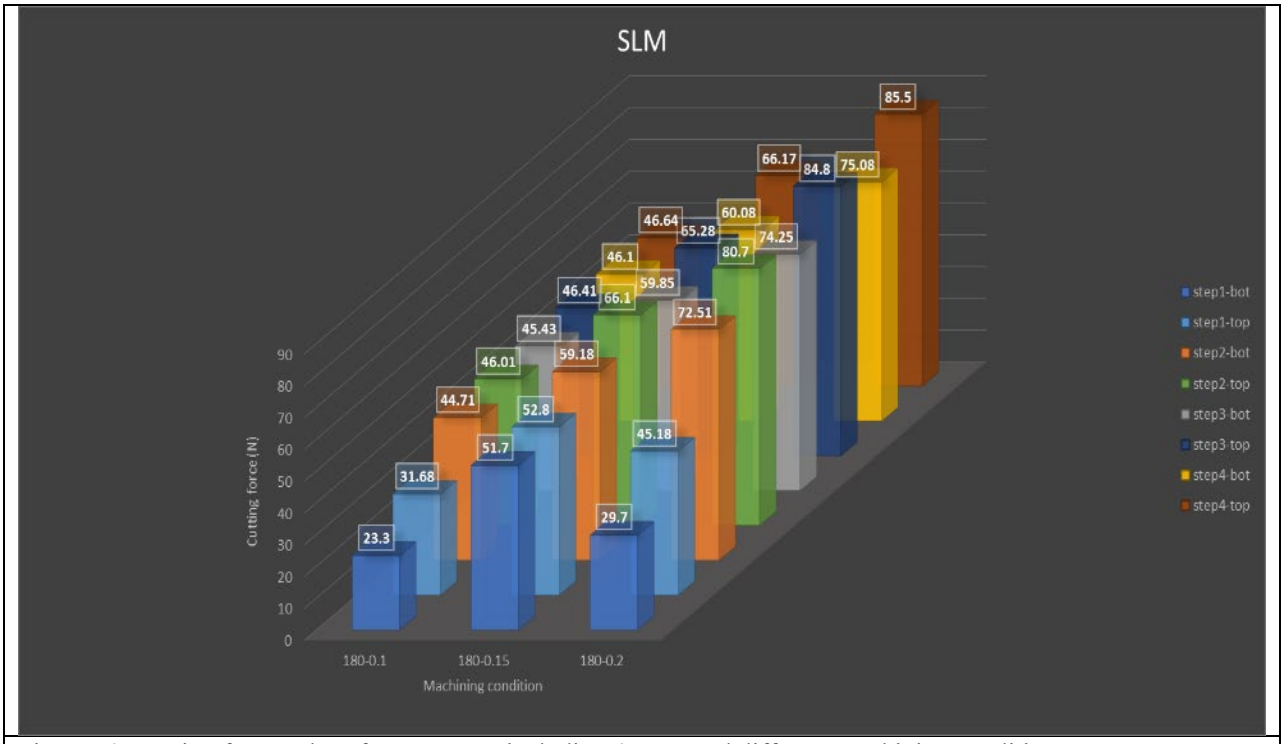

Figure 50: Cutting force values for SLM part including 4 steps and different machining conditions.

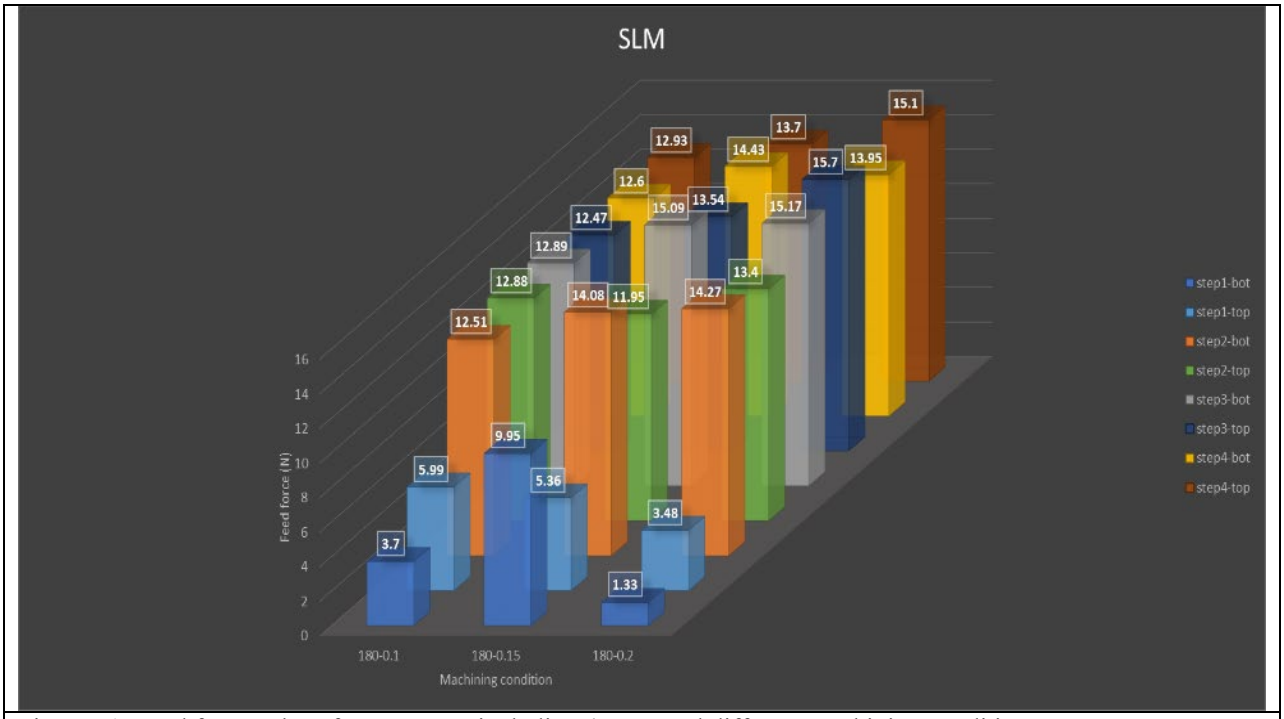

Figure 51: Feed force values for SLM part including 4 steps and different machining conditions.

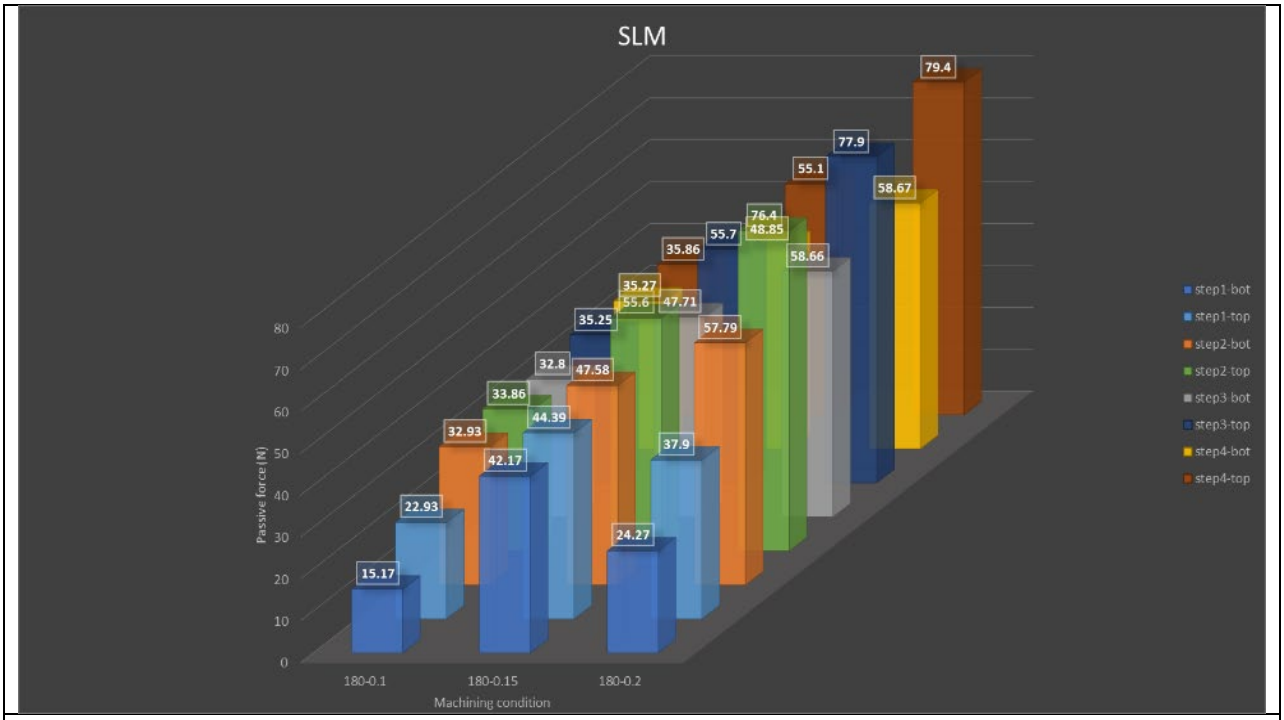

Figure 52: Passive force values for SLM part including 4 steps and different machining conditions.

At the bottom, the values of all three components of force in step 1 increase by moving from 0.1 to 0.15 and then decrease by moving from 0.15 to 0.2 mm/rev. However, the values of all force components in steps 2, 3 and 4 increase by moving from 0.1 to o.15 and then increase further to 0.2 mm/rev.

At the top, the value of cutting and passive components of force in step 1 increases by moving from 0.1 to 0.15 and then decreases by moving from 0.15 to 0.2 mm/rev. However, the values of all force components in steps 2, 3 and 4 increases by moving from 0.1 to o.15 and then further to 0.2 mm/rev except the feed force at step 2.

Roughness after machining

Roughness of all 4 steps after machining were measured by Sensofar optical profilometer instrument. The raw data were analyzed with Mountainsmap commercial software. The setup of the instrument is shown in figure 53. Roughness measurement after machining of additive manufactured component is reported in literature. However, the method of manufacturing is high-power direct laser deposition [2].

Figure 53: Set up of Sensofar optical profilometer for measuring roughness.

In SLM bottom surface the average roughness value (Sa) will be below 1 micron after step 1 up until step 4. Change of cutting speed will not affect the roughness values as shown in figure 54.

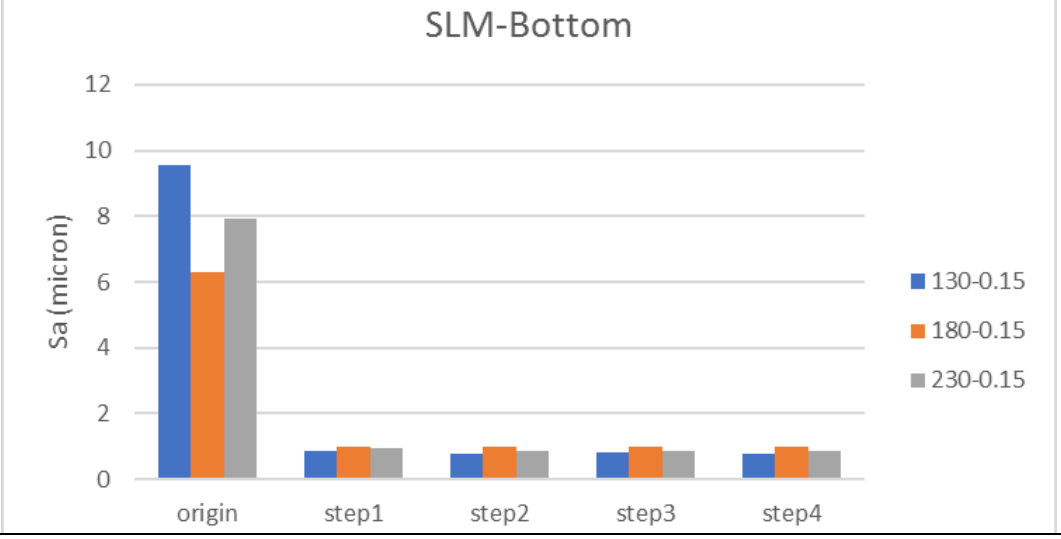

Figure 54: Average roughness values for the bottom part of SLM sample at 4 steps and different machining conditions.

In SLM top surface the average roughness will be around 1 micron after step 1 and continues to be the same until step 4. Change of cutting speed from 130 to 230 will not affect the roughness as shown in figure 55.

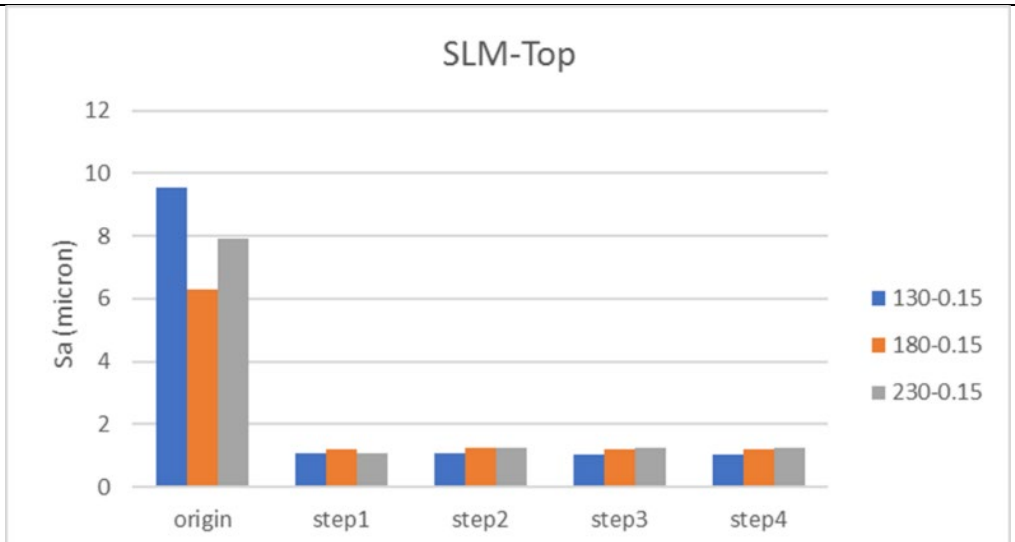

Figure 55: Average roughness values for the top part of SLM sample at 4 steps and different machining conditions.

In EBM bottom surface the average roughness will decrease at step 1 to a value of about 18 microns. After step 2 the values become slightly above 1 micron until step 4. However, the machining condition with cutting speed of 180 m/min will result in higher roughness at step 2 as shown in figure 56.

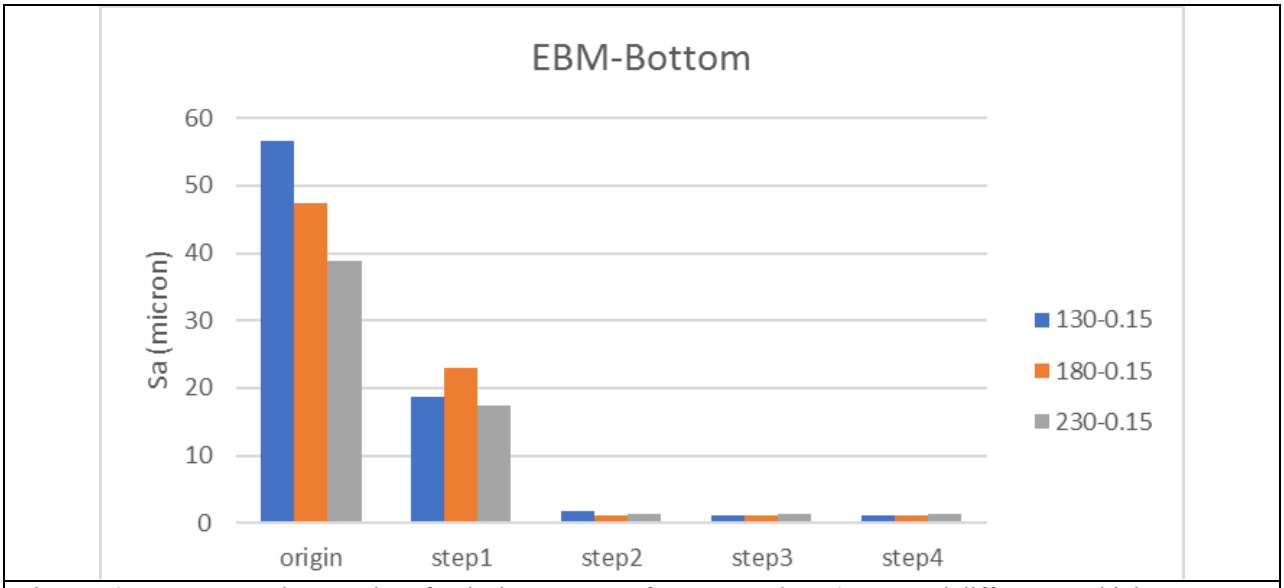

Figure 56: Average roughness values for the bottom part of EBM sample at 4 steps and different machining conditions.

In EBM top surface the average roughness will decrease faster with cutting speed of 180 m/min. However, the highest roughness is happening with cutting speed of 230 m/min as shown in figure 57.

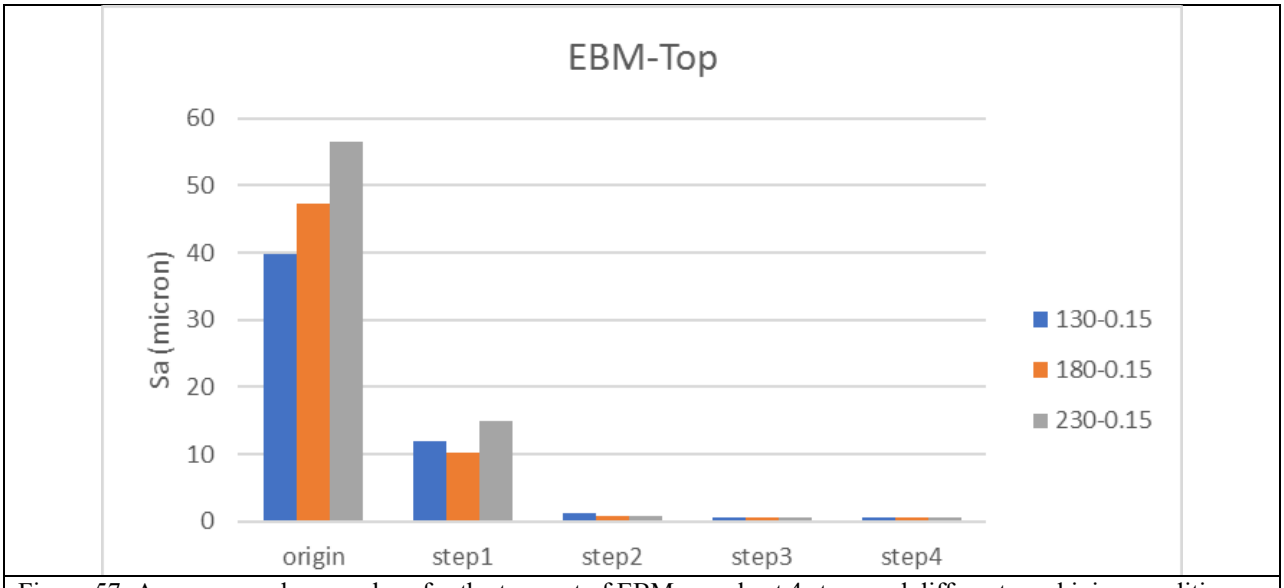

Figure 57: Average roughness values for the top part of EBM sample at 4 steps and different machining conditions.

Now we consider keeping the cutting speed constant at 180 m/min and varying the feed rate from 0.1 to 0.15 and to 0.2. This is valid just for SLM samples.

In SLM bottom surface the roughness values increase from feed rate of 0.1 toward feed rate of 0.15 and then to 0.2 mm/rev at all 4 steps. However, the roughness does not show changes from step 1 toward step 4 at a specific constant machining condition as shown in figure 58.

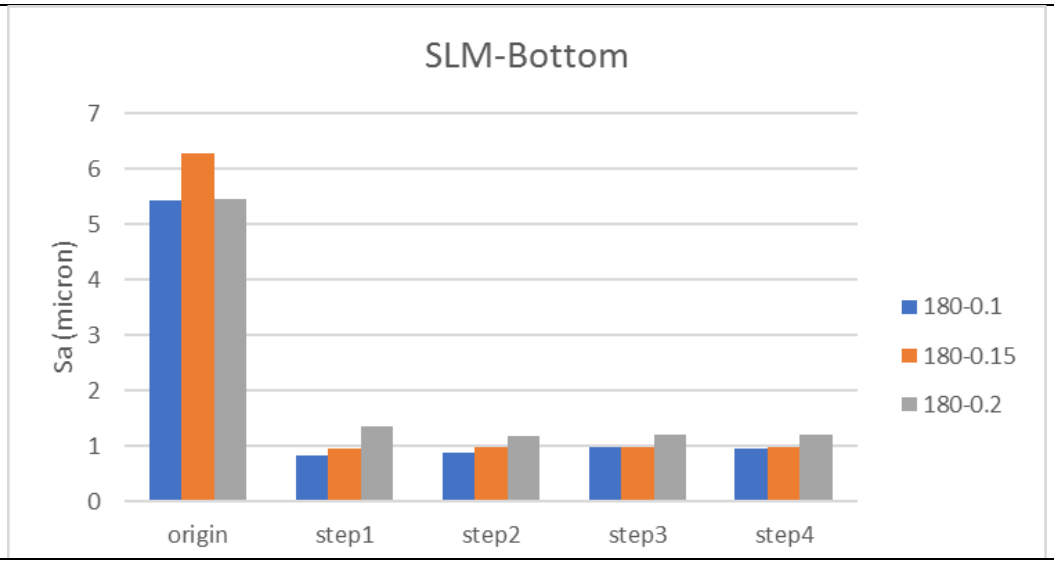

Figure 58: Average roughness values for the bottom part of SLM sample at 4 steps and different machining conditions.

The same trend of bottom surface is valid for top surface. It means that with increasing the feed rate from 0.1 to 0.2 mm/rev the average roughness will increase as shown in figure 59.

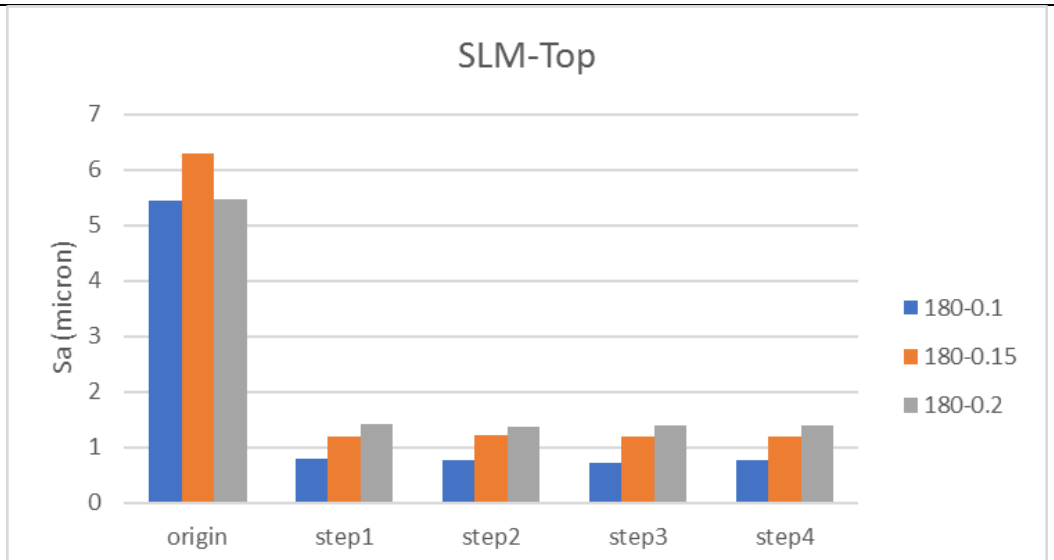

Figure 59: Average roughness values for the top part of SLM sample at 4 steps and different machining conditions.

Residual stress after machining

The residual stress at the bottom surface were measured at different depths from machined surface. The selected depths are 10, 20, 30, 50 and 100 microns as shown in figure 60. At first round of experiments, the etching of depths was done at circumference of the cylinder sample for each step. However, after precise measurements, we decided to etch at one point and going deeper and deeper until 100 micron is achieved. With new technique, we are sure that the correct depth is achived.

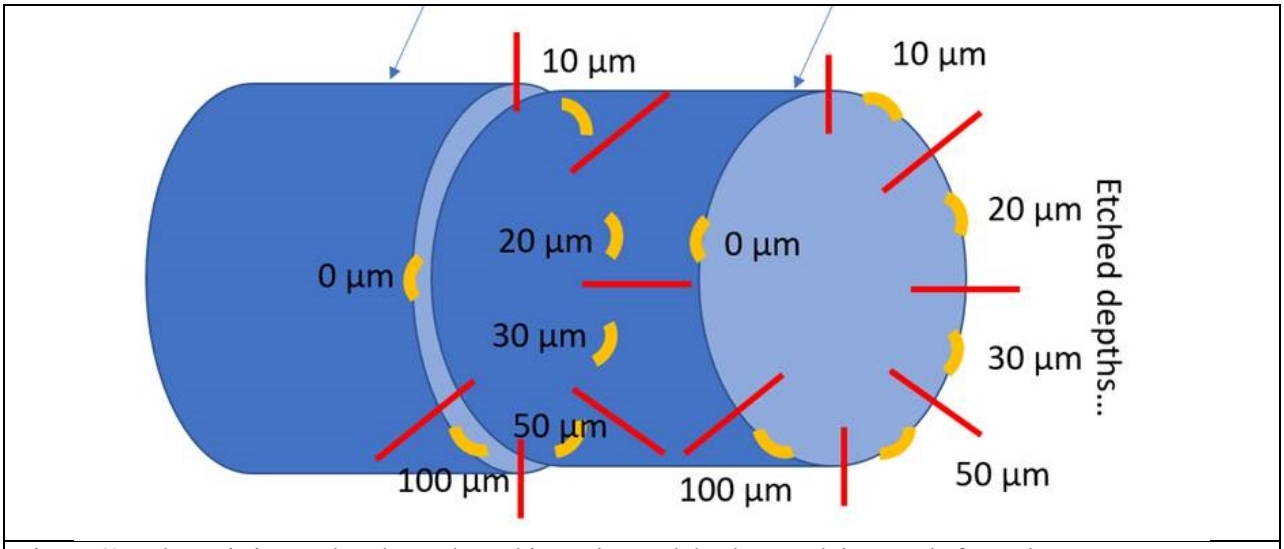

Figure 60: Schematic image that shows the etching points and depth around the sample for each step.

The electro-etching instrument from Struers was used to etch the samples to different depths. The etching tip is shown in figure 61.

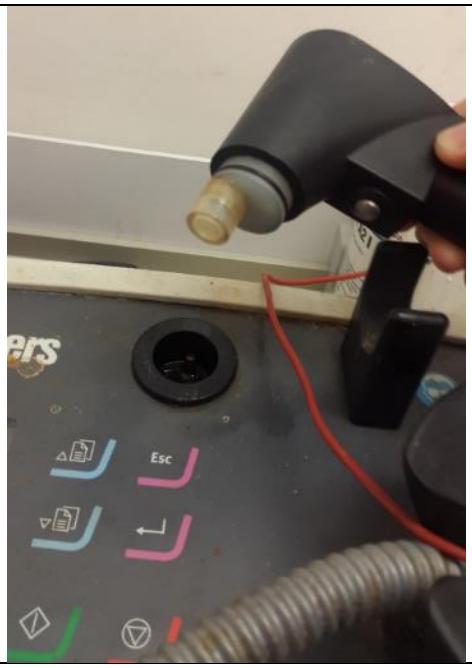

Figure 61: The etching tip from electro etching instruments of Struers.

Firstly, the etching depths measured with a manual profilometer, but the results were not correct. Therefore, we switched to optical profilometer for depth measurements. The etching depth profile measured with Sensofar optical profilometer is shown in figure 62. Since the depth profile is inclined so we considered the depth of middle point as the value for depth measurements.

Stress-tech X-ray robotic instrument was used to measure the residual stress as shown in figure 63.

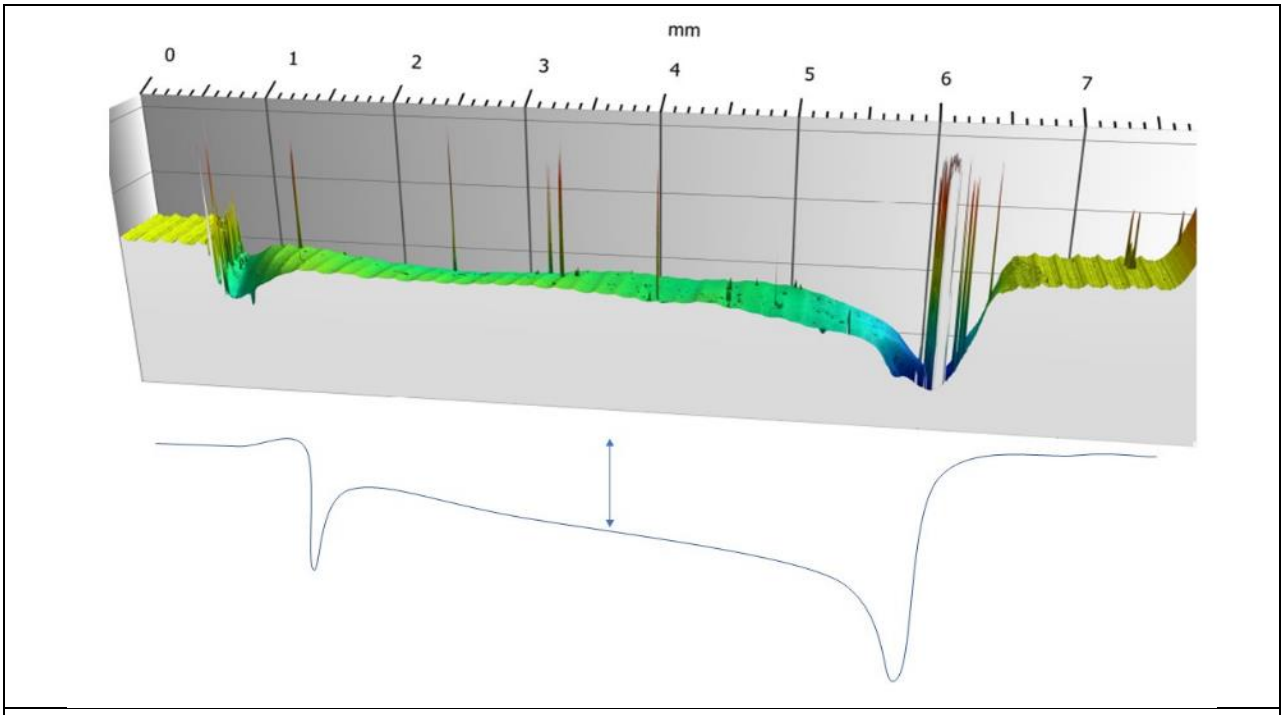

Figure 62: Etching depth profile from Sensofar instrument and the schematic one.

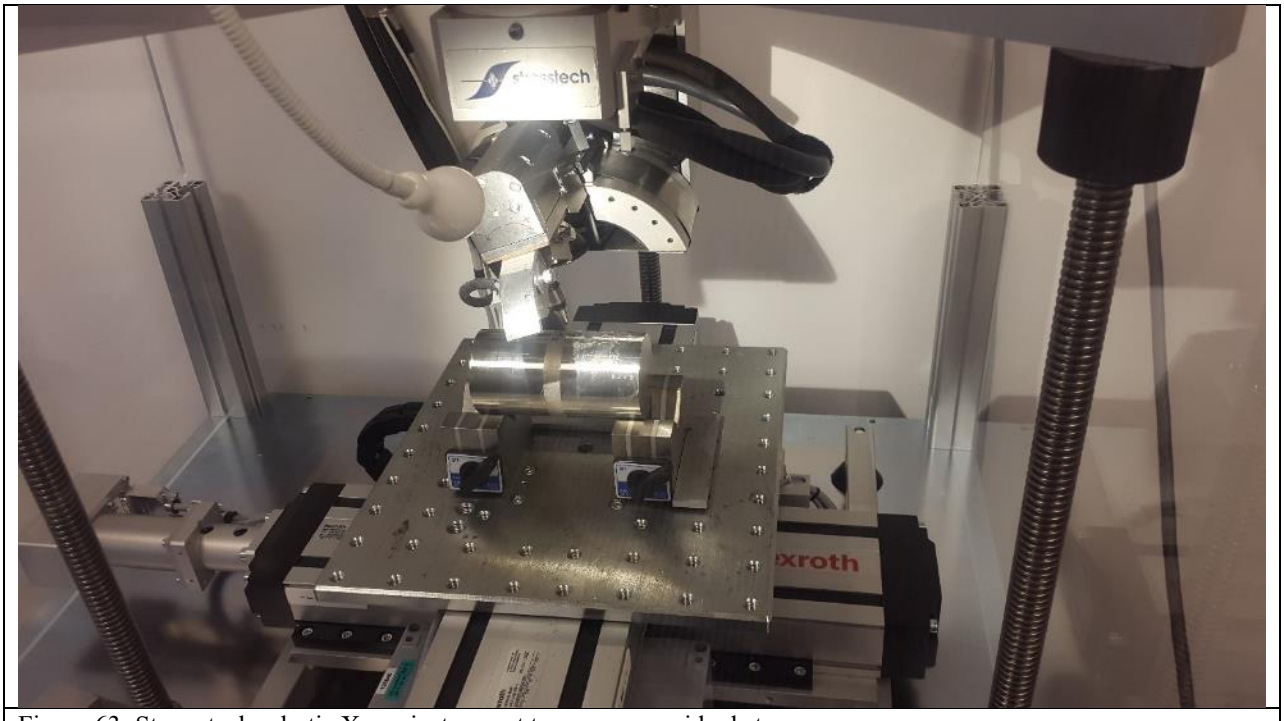

Figure 63: Stress-tech robotic X-ray instrument to measure residual stress.

The residual stress graph at step 1 and 4 of SLM sample at different depths from machined surface are shown in figures 64, 65. Residual stress measurements after machining are reported in literature [15,16].

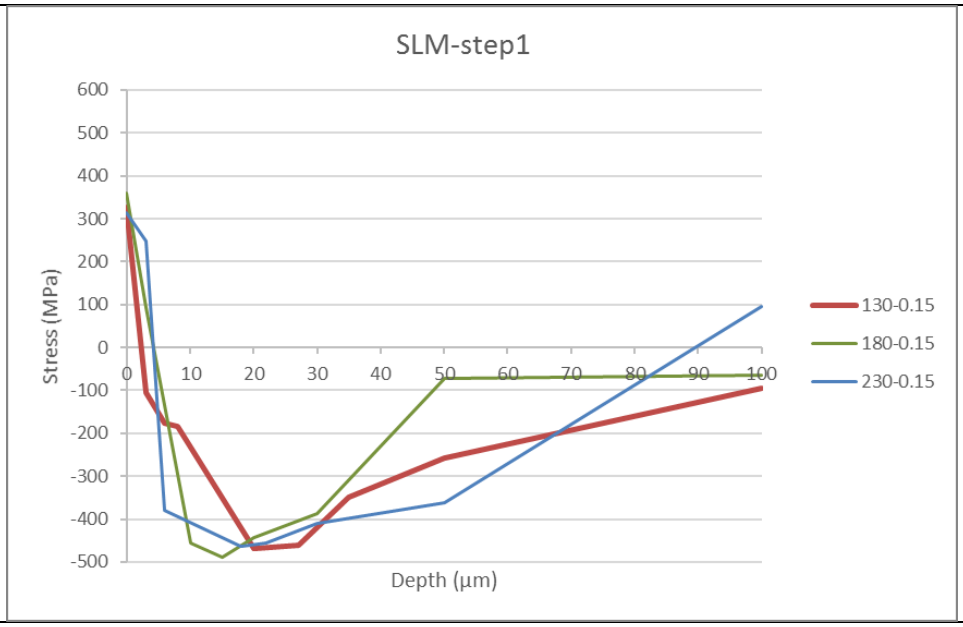

Figure 64: Residual stress values for step 1 of bottom part of SLM sample vs. depths at different machining conditions.

Figure 65: Residual stress values for step 4 of bottom part of SLM sample vs. depths at different machining conditions.

At first machined surface, the tensile stress values are higher in step 4 in comparison with step 1. However, the maximum compressive stress value is lower in step 4 in comparison with step 1. Maximum compressive stress happens between 10-30 micron under the machined surface.

The component after production with AM are under tensile stress due to rapid solidification of the last layer. However, machining will cause compressive stress under the surface. After certain depths, there will be tensile stress again in the sample. Tensile stress after additive manufacturing is reported in literature [17].

The residual stress graph at step 1 and 4 of EBM sample at different depths from machined surface are shown in figures 66, 67.

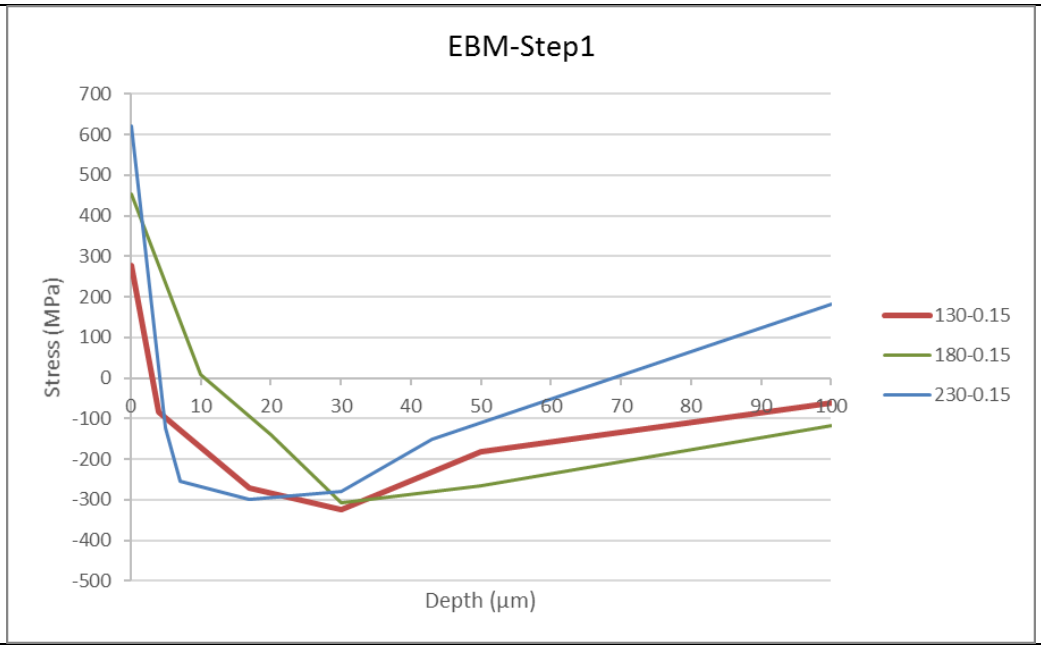

Figure 66: Residual stress values for step 1 of bottom part of EBM sample vs. depths at different machining conditions.

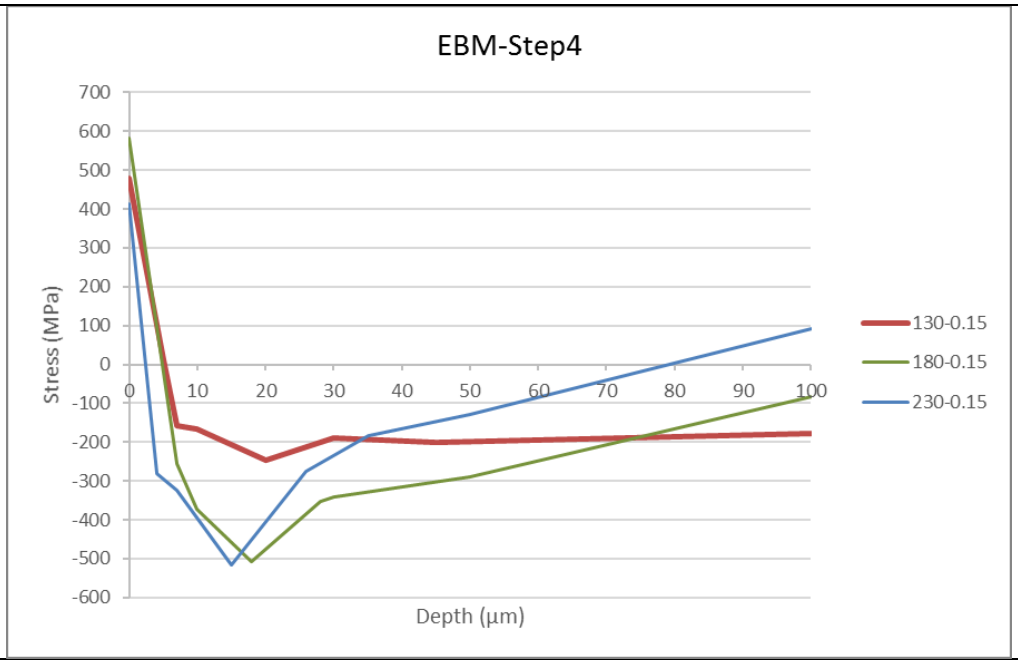

Figure 67: Residual stress values for step 4 of bottom part of EBM sample vs. depths at different machining conditions.

In both steps the maximum compressive stress happens at depth of 10 to 30 micron. The maximum compressive stress values in step 4 is higher than step 1 except for the machining condition of 130-0.15. With condition of 130-0.15, the machined surface is under higher tensile stress in step 4 in comparison with step 1 at the first machined surface (zero depth).

Conclusions

1) From SEM images, the melt pool sizes are about 250 microns in EBM and about 100 microns in SLM.
2) Cellular structure is evident in SLM but not in EBM samples. The cell sizes are about 0.5-1 micron in SLM samples.
3) From roughness measurements, the average surface roughness in EBM is about 9 times higher than in SLM in as-printed condition.
4) Hardness of SLM samples are about 30 Vickers higher than of the EBM samples.
5) EDX analysis of micron sized features in EBM shows that there are depletions of Fe, Cr, Ni, Mn within the features which can be due to lack of fusion.
6) In SLM after 0.25 mm depth of cut (1 passage) the surface quality is acceptable with average roughness of 0.8 micron.
7) In EBM after 0.75 mm depth of cut (3 passages) the surface quality is acceptable with average roughness of 0.9 micron.
8) 3 cutting passages in EBM is equal to removing 3 border layers.
9) Higher cutting forces of SLM samples at step 1 in comparison with EBM can be corresponding to higher hardness of SLM samples.
10) In SLM, at first machined surface, the tensile stress values are higher in step 4 in comparison with step 1. However, the maximum compressive stress value is lower in step 4 in comparison with step 1.
11) In EBM, the maximum compressive stress values in step 4 is higher than step 1 except for the machining condition of 130-0.15.
12) Maximum compressive stress happens between 10-30 micron under the machined surface in both SLM and EBM samples.
13) In additive manufacturing either by SLM or EBM, the component will remain under tensile stress after production. This is due to very rapid solidification of new layer in contact with the previous solid layer. Machining will cause compressive stress which balances the tensile stress to some certain depths.
14) With the intention of having the highest compressive stress, it is recommended to machine the surface for 1 step in SLM and 4 steps in EBM.

Future work

The future work will include the following:

- Measuring machining forces for top surfaces of EBM samples.
- Measuring the residual stress between steps 1 and 4.
- Measuring residual stress for top surfaces.
- Microstructure investigation of surfaces after machining and comparing them with as-printed condition.
- Measuring tool wear and correlating them with machining forces.

References

1) Struzikiewicz et al, Turning Research of Additive Laser Molten Stainless Steel 316L Obtained by 3D Printing, Materials, 2019, 12, p. 182.
2) Guo et al, Study on microstructure, mechanical properties and machinability of efficiently additive manufactured AISI 316L stainless steel by high-power direct laser deposition, Journal of materials processing technology, 2017, 240, p. 12-22.
3) Chen et al, Effect of heat treatment on microstructure, mechanical and corrosion properties of austenitic stainless steel 316L using arc additive manufacturing, Materials science and engineering A, 2018, 715, p. 307-314.
4) Yadollahi et al, Effects of process time interval and heat treatment on the mechanical and microstructural properties of direct laser deposited 316L stainless steel, Materials science and engineering A, 2015, 644, p. 171-183.
5) Saeidi et al, Transformation of austenite to duplex austenite-ferrite assembly in annealed stainless steel 316L consolidated by laser melting, Journal of alloys and compounds, 2015, 633, p. 463-469.
6) Saeidi et al, Hardened austenite steel with columnar sub-grain structure formed by laser melting, Materials science and engineering A, 2015, 625, p. 221-229.
7) Wang et al-Additively manufactured hierarchical stainless steels with high strength and ductility, Nature materials, 2017, p. 1-8.
8) Zhong et al, Intragranular cellular segregation network structure strengthening 316L stainless steel prepared by selective laser melting, Journal of nuclear materials, 2016, 470, p. 170-178.
9) Rannar et al, Hierarchical structures of stainless 316L manufactured by electron beam melting, Additive manufacturing, 2017, 17, p. 106-112.

10) Zhong et al, Additive manufacturing of ITER first wall panel parts by 2 approaches: selective laser melting and electron beam melting, Fusion engineering and design, 2017, 116, p. 24-33.
11) Roos et al, Macro and micromechanical behavior of 316LN lattice structures manufactured by electron beam melting, Journal of materials engineering and performance, 2019, p. 1-12.
12) Ryabov et al, Ratio of cutting force components in turning, Materials science forum, 2018, 940, p. 65-71.
13) Radovanovic et al, Correlation between components of cutting force by turning, Annals of the ORADEA university- Fascicle of management and technological engineering, 2006, 5, p. 1226-1231.
14) Lane et al, Post-process machining of additive manufactured stainless steel, ASPE spring topical conference, 2015.
15) Ganesh et al, Non-destructive micro-structural characterization of metallic specimens with a portable x-ray diffraction based residual stress analyzer, Studies in engineering and technology, 2015, 2, p. 22-32.
16) Outeiro et al, Machining residual stresses in AISI 316L steel and their correlation with the cutting parameters, Machining science and technology, 2002, 6, p. 251-270.
17) Simon et al, Residual stress measurements on AISI 316L samples manufactured by selective laser melting, Additive manufacturing, 2017, 17, p. 183-189.